Edinburgh Research Explorer

RNase H2, mutated in Aicardi-Goutières syndrome, promotes LINE-1 retrotransposition

Link:
Link to publication record in Edinburgh Research Explorer

Document Version:
Peer reviewed version

Published In:
EMBO Journal

RNase H2, mutated in Aicardi-Goutières syndrome, promotes LINE-1 retrotransposition

Maria Benitez-Guijarro[1,§], Cesar Lopez-Ruiz[1, #], Žygimantė Tarnauskaitė[2], Olga Murina[2], Mahwish Mian Mohammad[2,$], Thomas C. Williams[2], Adeline Fluteau[2], Laura Sanchez[1], Raquel Vilar-Astasio[1], Marta Garcia-Canadas[1], David Cano[1], Marie-Jeanne H. C. Kempen[2], Antonio Sanchez-Pozo[3], Sara R. Heras[1,3], Andrew P. Jackson[2], Martin A. M. Reijns[2,*] and Jose L. Garcia-Perez[1,2,*]

[1,]GENYO. Centro de Genómica e Investigación Oncológica: Pfizer-Universidad de Granada-Junta de Andalucía, Avenida de la Ilustración 114, PTS Granada, 18016 Granada, Spain

[2,]MRC Human Genetics Unit, MRC Institute of Genetics and Molecular Medicine, University of Edinburgh, Western General Hospital, Crewe Road, Edinburgh, EH4 2XU, United Kingdom

[3,]Department of Biochemistry and Molecular Biology II, Faculty of Pharmacy, University of Granada, Campus Universitario de Cartuja, 18071 Granada, Spain

[§,] Doctorate of Pharmacy Programme, The University of Granada, Granada, Spain.

[#]Present address: OncoMark Ltd., NovaUCD, Belfield Innovation Park, Dublin, Ireland

[$]Present address: CNRS - UMR 8200 - Institut Gustave Roussy, 94805 Villejuif, France

*Corresponding author: M.A.M.R. (e-mail: martin.reijns@igmm.ed.ac.uk) and J.L.G.-P. (e-mail: jose.garcia-perez@igmm.ed.ac.uk).

Keywords: Retrotransposition, LINE-1, Aicardi-Goutières Syndrome, RNase H2, TREX1, SAMHD1, ADAR1

Running Title: RNase H2 promotes L1 mobility

Final Character Count (excluding references): 79,568 characters (with spaces).

Abstract

Long INterspersed Element class 1 (LINE-1) elements are a type of abundant retrotransposons active in mammalian genomes. An average human genome contains ~100 retrotransposition-competent LINE-1s, whose activity is influenced by the combined action of cellular repressors and activators. TREX1, SAMHD1 and ADAR1 are known LINE-1 repressors and when mutated cause the autoinflammatory disorder Aicardi-Goutières syndrome (AGS). Mutations in RNase H2 are the most common cause of AGS and its activity was proposed to similarly control LINE-1 retrotransposition. It has therefore been suggested that increased LINE-1 activity may be the cause of aberrant innate immune activation in AGS. Here we establish that, contrary to expectations, RNase H2 is required for efficient LINE-1 retrotransposition. As RNASEH1 overexpression partially rescues the defect in RNase H2 null cells, we propose a model in which RNase H2 degrades the LINE-1 RNA after reverse transcription, allowing retrotransposition to be completed. This also explains how LINE-1 elements can retrotranspose efficiently without their own RNase H activity. Our findings appear to be at odds with LINE-1 derived nucleic acids driving autoinflammation in AGS.

Introduction

A significant proportion of most mammalian genomes consists of LINE-derived sequences, and the majority of these contain active LINE-1 (L1) elements. An average human genome contains more than 500,000 L1 copies but only 80-100 can currently mobilise (Beck et al, 2010; Brouha et al, 2003); these are termed retrotransposition-competent L1s or RC-L1s. As LINE-1 retrotransposition occurs randomly throughout the human genome, insertion events are sporadically mutagenic and can result in an array of genetic disorders ((Kazazian et al, 1988), reviewed in (Garcia-Perez et al, 2016; Hancks & Kazazian, 2012)). RC-L1s are 6-kb in length, contain an internal promoter in their 5'-UnTranslated Region (UTR) (Swergold, 1990), code for two intact Open Reading Frames (L1-ORF1p and L1-ORF2p), and end in a short 3'-UTR containing a variable sized poly-A tail required for retrotransposition (Doucet et al, 2015; Scott et al, 1987). L1-ORF1p is an RNA binding protein (Khazina & Weichenrieder, 2009) with nucleic acid chaperone activity (Martin & Bushman, 2001); L1-ORF2p codes for a protein with both Endonuclease (EN, (Feng et al, 1996)) and Reverse Transcriptase activities (RT, (Mathias et al, 1991), reviewed in (Richardson et al, 2015)). The enzymatic activities of L1-ORF1p and L1-ORF2p are strictly required for LINE-1 retrotransposition (Moran et al, 1996). In addition, L1-ORF2p contains a PCNA Interaction Protein motif (PIP) that allows interaction with PCNA (Proliferating Cell nuclear Antigen) and is required for efficient L1 retrotransposition (Taylor et al, 2013).

LINE-1 retrotransposition occurs by a mechanism termed Target Primed Reverse Transcription (TPRT, (Luan et al, 1993)). Briefly, upon transcription and translation of a full-length L1 mRNA (Alisch et al, 2006; Dmitriev et al, 2007; Swergold, 1990), both L1-encoded proteins bind to their own L1 mRNA in a process termed *cis*-preference (Wei et al, 2001), generating an L1 RiboNucleoprotein Particle (L1-RNP) that is considered a retrotransposition intermediate. Next, L1-RNPs access the nucleus by a process that does not require cell division (Kubo et al, 2006; Macia et al, 2017). In the nucleus, the L1 mRNA is reverse transcribed and integrated in a new genomic location by TPRT (Cost et al, 2002; Luan et al, 1993; Piskareva et al, 2003; Piskareva & Schmatchenko, 2006). During TPRT, L1-ORF2p recognizes and cleaves the bottom strand of genomic DNA in a consensus sequence (5´TTTT/AA and variants, (Jurka, 1997)), generating a free 3´OH that is used by the RT activity of L1-ORF2p to prime first-strand cDNA synthesis. As a result, an L1 RNA:cDNA hybrid covalently linked to the genome is generated. The mechanism of second-strand cDNA synthesis is not fully understood, but requires removal of the L1 mRNA from the generated hybrid, which allows second strand cDNA synthesis to occur. In this context, there are two main classes of LINE elements: elements coding for a functional RNase H domain (mostly present in plants and lower eukaryotes) and elements that lack

this domain (most mammals, including human LINE-1s) (Malik et al, 1999; Olivares et al, 2002; Piskareva & Schmatchenko, 2006). RNase H enzyme activity degrades the RNA strand of RNA:DNA heteroduplexes, and how LINE elements without a functional RNase H domain achieve this is currently not known. Either way, it is assumed that upon removal of the LINE mRNA from the hybrid, the top strand of genomic DNA is cleaved, presumably by L1-ORF2p, releasing a 3´OH that is then used to prime second strand cDNA synthesis, also presumed to be carried out by L1-ORF2p (Cost et al, 2002; Piskareva et al, 2003; Piskareva & Schmatchenko, 2006) (reviewed in (Richardson et al, 2015)). The result of TPRT is the generation of a new LINE-1 insertion, usually flanked by short Target Site Duplications (TSDs) and often 5'-truncated (Richardson et al, 2015).

Due to their mutagenic potential, the host has evolved a myriad of mechanisms to control LINE-1 expression and retrotransposition (recently reviewed in (Garcia-Perez et al, 2016; Heras et al, 2014; Pizarro & Cristofari, 2016)). Some repressors of L1 activity, when mutated, were shown to cause rare genetic disorders, such as Ataxia Telangiectasia (Coufal et al, 2011) and Aicardi-Goutières syndrome (AGS, reviewed in (Volkman & Stetson, 2014)). AGS is a type I interferonopathy where aberrant innate immune activation causes type I IFN production and clinical features reminiscent of a congenital viral infection of the brain (Crow & Manel, 2015). AGS is caused by mutations in one of seven genes: the 3´exonuclease TREX1 (Crow et al, 2006a), the deoxynucleoside triphosphate triphosphohydrolase and putative ribonuclease SAM domain and HD domain 1 (SAMHD1) (Rice et al, 2009), the adenosine deaminase acting on RNA 1 (ADAR1) (Rice et al, 2012), the dsRNA cytosolic sensor IFN-induced helicase C domain containing protein 1 (IFIH1) (Rice et al, 2014) and the three subunits of the ribonuclease H2 (RNase H2) endonuclease complex (RNASEH2A, RNASEH2B and RNASEH2C) (Crow et al, 2006b) (reviewed by (Crow & Manel, 2015). In most cases, the IFN response in AGS patients is likely the consequence of the accumulation of aberrant cytoplasmic nucleic acids that activate innate immune receptors. Although the nature of such immunostimulatory nucleic acids has not been fully characterized, retrotransposons have been proposed as a possible source (Volkman & Stetson, 2014). In line with this, TREX1, SAMHD1 and ADAR1 have been shown to inhibit the mobility of LINE-1s (Orecchini et al, 2017; Stetson et al, 2008; Zhao et al, 2013), and RNase H2, mutated in more than half of all known AGS patients (Crow et al, 2015), was suggested to similarly control LINE-1 retrotransposition (Volkman & Stetson, 2014).

Mammalian cells have two enzymes with the ability to degrade the RNA strand of RNA:DNA heteroduplexes: RNase H1 and RNase H2 (reviewed by (Cerritelli & Crouch, 2009)). RNase H1 has two isoforms, one localises to mitochondria and is essential for

mitochondrial DNA replication (Cerritelli et al, 2003), the second is nuclear and important for preventing R-loops and consequent transcription-replication conflicts (Nguyen et al, 2017; Parajuli et al, 2017; Shen et al, 2017). RNase H2, a heterotrimeric complex, is the predominant nuclear enzyme responsible for RNA:DNA hybrid degradation (reviewed by (Reijns & Jackson, 2014)), although this may depend on cell type. RNase H2 is essential for genome stability, and also has the ability to cleave the 5'-phosphodiester bond of ribonucleotides embedded in a DNA duplex, an activity required for the removal of misincorporated ribonucleotides (Hiller et al, 2012; Nick McElhinny et al, 2010; Reijns et al, 2012) in a process called ribonucleotide excision repair or RER (Sparks et al, 2012). Whereas the catalytic core of RNase H2 is present in the RNASEH2A subunit, all three subunits are required for its activity (Reijns & Jackson, 2014). The precise role for the accessory RNASEH2B and C subunits is not well understood, but a functional PCNA-interacting PIP motif is found in RNASEH2B (Chon et al, 2009), directing RNase H2 activity to replication and repair foci (Bubeck et al, 2011; Kind et al, 2014).

Here, we analyse the role of RNase H2 in LINE-1 retrotransposition and find that, in contrast to other AGS proteins, RNase H2 enzyme activity facilitates human LINE-1 retrotransposition. In the absence of RNase H2, overexpression of RNase H1 partially rescues the LINE-1 retrotransposition defect. Furthermore, overexpression of wildtype RNase H2 or a separation of function mutant of RNase H2 that can only cleave RNA:DNA heteroduplexes results in increased LINE-1 retrotransposition. The requirement for RNase H2 appears to be specific to retroelements without their own RNase H domain, suggesting that cellular RNase H activity is necessary to degrade the LINE-1 RNA in the RNA:cDNA hybrid generated during retrotransposition. Our findings call into question the existence of a unifying molecular mechanism for AGS pathogenesis centred around the accumulation of LINE-1 nucleic acids.

Results

LINE-1 retrotransposition is compromised in RNase H2 null HeLa cells

To test the effect of RNase H2 on LINE-1 retrotransposition, we generated a panel of clonal HeLa RNase H2 null cell lines using CRISPR/Cas9 mediated genome editing and guide RNAs (gRNAs) directed to the RNASEH2A subunit (Fig 1). Individual mutant clones were selected based on deletions/insertions observed after PCR amplification and sequencing of the target locus. Loss of RNASEH2A expression and reduced levels of RNASEH2B and C were shown by Western analysis in knockout clones (KO, Fig 1A). Additionally, loss of RNase H activity in cell lysates against single embedded ribonucleotides was confirmed using a FRET-based fluorescent substrate release assay (Fig 1B). Finally, increased fragmentation of genomic DNA from KO clones after RNase H2 treatment and alkaline gel electrophoresis indicated the presence of large numbers of embedded ribonucleotides in KO clones (Fig 1C), a well-known consequence of RNase H2 deficiency (Hiller et al, 2012; Nick McElhinny et al, 2010; Reijns et al, 2012). For these and subsequent experiments, KO clones were compared to parental cells as well as CRISPR control clones (C) that retained significant RNase H2 activity.

These RNase H2 null and control clones were used in a cell-based LINE-1 mobilization assay, which makes use of an active human LINE-1 element (L1.3, (Sassaman et al, 1997)) tagged with a reporter gene that can only be activated after a round of retrotransposition (Fig 1D and EV1A, (Moran et al, 1996)). As a reporter gene we used *mblastI* (Goodier et al, 2007; Morrish et al, 2002), which activates the Blasticidin resistant gene after retrotransposition (Fig 1D, plasmid JJ101/L1.3). Importantly, this assay is quantitative, and the resulting number of drug-resistant colonies provides a readout of retrotransposition activity (Goodier et al, 2007; Morrish et al, 2002). Surprisingly, LINE-1 retrotransposition was severely reduced in the RNase H2 null lines (*n* = 6 clones), with an average level of retrotransposition of 6.0±2.6% (mean ± SD) compared to control lines (*n* = 6, 94±22%; *P* = 0.0022) or parental cells (set to 100%) (Fig 1E, F). As expected, control plasmids containing RT mutated LINE-1 (JJ101/L1.3-D702A) failed to retrotranspose in all cell lines (Fig 1F), whereas similar numbers of blasticidin-resistant colonies were generated for all cell lines after transfection with a control vector (pcDNA6.1, expressing the blasticidin resistant gene, Fig EV1B). Retrotransposition of an EN mutant LINE-1 (JJ101/L1.3-D205A) was similarly low in wild type and null cells, suggesting that DNA lesions in null cells (Reijns et al, 2012) are not used as integration sites by endonuclease mutant LINE-1 (Fig 1F).

To confirm these data, we next used an L1 retrotransposition assay that activates expression of luciferase upon retrotransposition (Fig EV1C). This assay has two

advantages over the drug-resistance based assay: i) it does not require selection with antibiotic or generation of drug-resistant colonies, and ii) retrotransposition levels are measured 96 h post-transfection. This way long-term culturing is avoided, and possible confounding effects due to differential growth between controls and RNASEH2A-KO cell lines can therefore be ruled out. Using this luciferase-based assay we observed a 63% reduction in L1 retrotransposition in RNase H2 null cell lines (n = 3, 31±6.2%) compared to controls (n = 3, 84±8.3%; P = 0.0009; Fig EV1D). Furthermore, to exclude an indirect effect of RNase H2 deficiency on L1 expression, we performed Western blot analysis using an antibody against endogenous L1-ORF1p. Although there was some variation between clones, we confirmed that L1-ORF1p is expressed at similar levels in RNASEH2A-KO cells and parental cells (Fig EV1E-G). In summary, these data suggest that RNase H2 promotes LINE-1 retrotransposition in cultured HeLa cells.

LINE-1 retrotransposition is compromised in RNase H2 null U2OS and HCT116 cells

To determine if RNase H2 activity is required for LINE-1 mobilization in other cellular backgrounds, we next analysed retrotransposition in colon carcinoma (HCT116) and osteosarcoma (U2OS) cells. Firstly, using the same CRISPR/Cas9 strategy, we generated RNASEH2A-KO and control clones using HCT116 p53$^{-/-}$ cells. Western blotting, enzyme activity assays and analysis of genomic ribonucleotide incorporation confirmed absence of RNase H2 activity in two clonal knockout cell lines (KO, Appendix Fig S1A-C). Using the JJ101/L1.3-based assay, we observed significantly reduced retrotransposition in HCT116 RNASEH2A-KO clones (n = 2, 29±8.5%) compared to controls cells (n = 4, 100±14%, P = 0.0028) (Appendix Fig S1D, E).

Secondly, we generated clonal RNASEH2A-KO and control lines using U2OS cells (Fig 2A-C), which were assayed for retrotransposition alongside parental cells. Notably, and consistent with our data for HeLa and HCT116 p53$^{-/-}$ RNase H2 null cells, we observed a substantial reduction in LINE-1 retrotransposition in the RNASEH2A-KO lines (n = 2, 25±9.5%) compared to parental cells (set to 100%) and a wildtype control clone (n = 2, 94±8.2%; P = 0.016) (Fig 2D). Additional controls showed that all clones generated similar number of blasticidin-resistant colonies upon transfection with the control vector pcDNA6.1, and that an L1 RT mutant construct (L1.3-D702A) failed to retrotranspose in all U2OS clones tested (Fig 2D).

In summary, LINE-1 retrotransposition is strongly reduced in multiple RNase H2 null clones of three different cell lines. We therefore conclude that cellular RNase H2 activity is required for efficient LINE-1 retrotransposition.

RNase H2 facilitates mobilization of non-LTR retroelements but is dispensable for LTR-retrotransposons and DNA-Transposons

During LINE-1 insertion by Target Primed Reverse Transcription (TPRT), after endonucleolytic cleavage of genomic DNA and first strand cDNA synthesis by L1-ORF2p, an L1 RNA:cDNA hybrid attached to the genome is generated. The RNA in the hybrid must be removed prior to starting second strand cDNA synthesis. Because human L1-ORF2p lacks RNase H activity (Cost et al, 2002; Malik et al, 1999; Mathias et al, 1991; Piskareva et al, 2003; Piskareva & Schmatchenko, 2006), we reasoned that cellular RNase H2 may instead degrade the RNA in the L1 RNA:cDNA hybrid. To test if RNase H2 performs this function more generally for LINE elements lacking an RNase H domain, we next investigated the impact of RNase H2 deficiency on retrotransposition of a LINE-2 element from zebrafish (ZfL2-2). Notably, ZfL2-2 does not contain an RNase H domain and is active in human cells lines (Garcia-Perez et al, 2010; Sugano et al, 2006). We tagged this LINE-2 element with an *mneoI* retrotransposition indicator cassette, which confers resistance to neomycin/G418 upon retrotransposition (Freeman et al, 1994; Moran et al, 1996) (Fig 3A), and measured activity in the HeLa RNASEH2A-KO and control clones. An active human LINE-1 tagged with the same retrotransposition indicator cassette (vector JM101/L1.3, Fig 3A) was used in parallel as a control. The JM101/L1.3-*mneoI* vector produced results very similar to JJ101/L1.3-*mblastI* (Fig 1 and 3C). Consistent with our hypothesis, ZfL2-2-*mneoI* retrotransposition was significantly reduced in null clones (n = 5, 1.6±0.91%) compared to parental cells (set to 100%) and control clones (n = 5, 85±9.5%; P = 0.0079) (Fig 3A-C and EV2A). Notably, when ZfL2-2 was assayed in the U2OS RNASEH2A-KO and control clones, we observed a virtually identical outcome (Fig EV2B; n = 2 controls, 105±3.5% vs n = 2 KO, 14±2.4%; P = 0.0012). As expected, we detected a similar reduction in the retrotransposition rate of a human LINE-1 element in both HeLa and U2OS RNASEH2A-KO clones using the *mneoI*-based assay (Fig 3A-C and EV2). Taken together, these data suggest that LINE elements lacking a functional RNase H domain rely on cellular RNase H2 activity to retrotranspose efficiently. This would make RNase H2 an integral part of the LINE retrotransposition machinery.

In line with this model, we reasoned that retrotransposons that do contain a functional RNase H domain would not rely on cellular RNase H2 activity to retrotranspose efficiently. Active LTR-retrotransposons from the mouse genome contain a functional RNase H domain within their *pol* gene (Doolittle et al, 1989); they generate cytoplasmic RNA:cDNA hybrid intermediates during their retrotransposition cycle, with RNA degradation required to complete LTR-retrotransposition. We therefore measured retrotransposition of MusD, an

active LTR-retrotransposon from the mouse genome (Doolittle et al, 1989; Mager & Freeman, 2000). To do so, we tagged an active MusD element with the neo[TNF] retrotransposition indicator cassette (pCMVMusD-6 neoTNF; Fig 3D, Appendix Fig S2A; (Ribet et al, 2004)) and tested its activity in RNASEH2A-KO and control clones. Consistent with our model, the level of MusD retrotransposition was similar in HeLa control and RNASEH2A-KO clones (Fig 3D, Appendix Fig S2B). Similarly, no difference in MusD activity was observed either when comparing U2OS RNase H2 wildtype and null cells (Appendix Fig S2C). Thus, these data strongly suggest that retrotransposons containing a functional RNase H domain do not depend on cellular RNase H2 activity for their mobilization.

We next tested whether mobilisation of DNA-Transposons, that move by a cut-and-paste mechanism that does not involve Reverse Transcription, would require cellular RNase H2 activity. We employed an active Tc1-like resurrected DNA-Transposon termed Sleeping Beauty (SB) (Ivics et al, 1997) that transposes very efficiently in human cells. Using an SB transposition assay based on G418 selection, no differences in transposition rates were observed when comparing RNase H2 null clones and controls, for either HeLa (Fig 3E) or U2OS (Appendix Fig S2D) cell lines.

We therefore conclude that neither LTR-retrotransposons that code for RNase H activity, nor DNA-Transposons, rely on cellular RNase H2 activity for their mobilisation.

RNase H2 overexpression increases LINE-1 retrotransposition

If RNase H2 is directly required for LINE-1 retrotransposition it may be expected that overexpression of RNase H2 might further increase retrotransposition efficiency, and we set out to test this. RNase H2 is a heterotrimeric enzyme, and overexpression of the catalytic subunit alone does not significantly increase cellular activity (KR Astell, MAM Reijns & AP Jackson, unpublished data). We therefore co-transfected HeLa and U2OS cells with three plasmids each expressing one of the RNase H2 subunits tagged with a V5 epitope tag and an engineered human LINE-1 construct tagged with the *mblastI* indicator cassette (JJ101/L1.3). As controls, we transfected cells with a β-arrestin expression vector, a negative control (-ve) that does not significantly affect L1 retrotransposition (Bogerd et al, 2006), or with an APOBEC3A overexpression vector, a positive control (+ve) that strongly inhibits LINE-1 retrotransposition (Bogerd et al, 2006; Richardson et al, 2014). Cells were also co-transfected in a parallel assay with the control vector pcDNA6.1, and resulting colony numbers used for normalisation to control for potential toxic side effects of cDNA overexpression. Notably, when HeLa or U2OS cells were co-transfected with equal

amounts of overexpression plasmid for each RNase H2 subunit (ratio 1:1:1) and vector JJ101/L1.3, we detected a significant increase in retrotransposition when compared to the β-arrestin control (2.1-fold in HeLa and 1.7-fold in U2OS, Fig 4). In agreement with previous reports (Bogerd et al, 2006), overexpression of APOBEC3A reduced LINE-1 retrotransposition to ~10% of control levels (Fig 4, (Bogerd et al, 2006)). As expected, RT mutant LINE-1s failed to retrotranspose in any condition tested and the retrotransposition of EN mutant LINE-1s was not affected by RNase H2 overexpression (Fig 4), suggesting that RNase H2 cleavage at misincorporated ribonucleotides does not provide an entry point for endonuclease mutant LINE-1s. Western blot analysis showed that the three V5-tagged RNase H2 subunits were expressed, although they were not detected at the same level (Fig EV3A). Through optimisation, we found that a 14:7:1 transfection ratio (for RNASEH2A, B and C respectively) produced the most similar expression levels for each of the subunits (Fig EV3A). When measuring retrotransposition at this 14:7:1 ratio, LINE-1 retrotransposition increased again, this time by ~1.7-fold for HeLa cells and ~1.4-fold for U2OS cells (Fig EV3B, C). Thus, rather than reduced LINE-1 retrotransposition being an indirect effect of RNase H2 deficiency, these data are consistent with a direct role for cellular RNase H2 in facilitating LINE-1 retrotransposition.

Complementation of KO cells with wildtype, but not separation of function RNASEH2A rescues LINE-1 retrotransposition

RNase H2 can cleave at ribonucleotides embedded in double stranded DNA, and can hydrolyse the RNA strand of RNA:DNA heteroduplexes, raising the question as to which of these two activities is required to promote LINE-1 retrotransposition. Elegant work in yeast identified two amino acid changes in the RNase H2 catalytic subunit that severely abrogates its activity against single embedded ribonucleotides, while retaining activity against RNA:DNA heteroduplexes (Chon et al, 2013). We took advantage of this "separation of function" (SoF) mutant to try to address this question (Fig EV4A). First, we tested whether the biochemical characteristics of recombinant human RNase H2 with the equivalent mutations (P40D/Y210A) were similar to that of the yeast enzyme (Fig 5A-D, and (Chon et al, 2013)). As expected, recombinant human SoF RNase H2 has virtually no activity against single embedded ribonucleotides (Fig 5A, B), but retains activity against RNA:DNA heteroduplexes (Fig 5C, D). However, activity against RNA:DNA heteroduplex substrate was reduced compared to wildtype RNase H2, and unexpectedly, we also found that the SoF mutant produced longer RNA products when compared to wildtype RNase H2 (Fig 5C), suggestive of an altered cleavage pattern. This difference in cleavage was

observed even with higher enzyme concentrations and at longer incubation times (Fig EV4B).

We next complemented a HeLa RNASEH2A-KO clone (KO1) using retroviral vectors to generate stable cell lines expressing either wildtype or SoF RNASEH2A. Cell lines expressing the empty vector (EV) or catalytically inactive (Catalytic dead, CD) RNASEH2A (D34A/D169A; (Reijns et al, 2011)) were also generated and used as controls. Western blotting confirmed expression of RNASEH2A and the consequent stabilisation of RNASEH2B and C in complemented cells at levels indistinguishable from control cells (Fig 5E). As expected, complementation with WT RNASEH2A but not EV, SoF or CD reduced the level of ribonucleotide incorporation to a level similar to that observed in wildtype controls (Fig EV4C). This was consistent with the level of RNase H activity against single embedded ribonucleotides measured in cell lysates in complemented cells (Fig 5F and EV4D, E). On the other hand, activity against RNA:DNA heteroduplexes was similar for the WT complemented cells (+WT) and wildtype control cells (C1), whereas the SoF complemented cells displayed <50% activity (Fig 5G and EV4F,G), in line with the observed reduction in activity of recombinant SoF RNase H2. RNase H1 is expressed in all of these cells, explaining the residual activity against RNA:DNA substrate in RNASEH2A-KO cells complemented with empty vector or RNASEH2A-CD. Notably, the altered cleavage pattern on RNA:DNA hybrids was also detected in cell lysates from RNASEH2A-SoF complemented cells (Fig EV4G). These data suggest that, although the P40D/Y210A amino acid changes in human RNase H2 do act as separation of function mutations, RNase H activity against RNA:DNA heteroduplexes of the SoF mutant is compromised both *in vitro* and *in vivo*.

Retrotransposition assays on the complemented cell lines using vector JJ101/L1.3 demonstrated that complementation with wildtype RNASEH2A allowed efficient retrotransposition (Fig 5H). A second HeLa RNASEH2A-KO clone (KO2) complemented with WT RNASEH2A also showed rescue of the L1-retrotransposition defect (Fig EV4H), confirming that reduced retrotransposition in RNASEH2A-KO cells is due to lack of RNase H2 activity and not due to potential off-target effects of CRISPR/Cas9. In contrast, complementation with RNASEH2A-SoF failed to rescue the L1 retrotransposition defect, with levels similar to those seen in EV or CD complemented cells (Fig 5H). Failure to complement the LINE-1 retrotransposition defect in RNase H2 null cells with the RNASEH2A separation of function mutant may be a direct consequence of its altered biochemical characteristics, resulting in its failure to fully/efficiently degrade the RNA in the LINE-1 RNA:cDNA hybrid. However, it is formally possible that RNase H2 promotes LINE-1 retrotransposition through its activity on embedded ribonucleotides.

No increased mutation rates in newly inserted LINE-1 elements in RNase H2 null cells

It has been shown that during Human Immunodeficiency virus type 1 (HIV-1) reverse transcription, ribonucleotides are misincorporated at high frequency by the RT of HIV-1, especially in macrophages (Kennedy et al, 2012). Notably, RNase H2 was shown in a high throughput screen to be important for HIV-1 infection (Genovesio et al, 2011), and it may be involved in removing such embedded ribonucleotides. Although drastic differences exist among the mechanism of retroviral insertion and LINE-1 retrotransposition, it is therefore possible that ribonucleotides are misincorporated during L1 reverse transcription and/or second strand synthesis, and that their removal by RNase H2-dependent RER is important to allow efficient retrotransposition to occur. Ribonucleotide misincorporation in RNase H2 deficient yeast was shown to cause high rates of Top1-dependent 2-5 bp deletions (Kim et al, 2011; Nick McElhinny et al, 2010). These mutations are most likely to occur at tandem dinucleotide repeats, particularly CA:TG and GA:TC (Clark et al, 2011; Kim et al, 2013; Kim et al, 2011; Potenski et al, 2014). These repeats occur in our retrotransposition reporters at rates similar to the yeast reporters, and as such mutations are likely to inactivate the drug selectable marker used in our assays, this could explain the apparent reduction in retrotransposition in RNase H2 null cells. We therefore set out to determine the occurrence of such mutations in newly inserted LINE-1 elements in RNase H2 null and control cells. To do this, we transfected plasmid JM101/L1.3, containing the *mneoI* retrotransposition cassette, into RNase H2 null HeLa clones (KO1 and KO2) and parental cells, and allowed cells to grow for 5 days without G418 selection (Appendix Fig S3A, B). Two and five days after transfection, genomic DNA was isolated and analysed by conventional PCR, using intron-spanning primers and thus allowing us to distinguish retrotransposed products (shorter amplification products) from the transfected vector (Appendix Fig S3A, C). Sequencing of amplification products corresponding to the spliced *mneoI* reporter (i.e. *de novo* L1 insertions) showed no increase in mutations in RNASEH2A-KO cells compared to RNase H2 proficient cells (Appendix Fig S3D, E). Notably, only missense mutations were identified, with no 2-5 bp deletions detected in any of the clones analysed. We therefore conclude that the LINE-1 retrotransposition defect in RNase H2 null cells is not caused by hypermutation of *de novo* L1 insertions that could result from failure to remove ribonucleotides misincorporated during TPRT.

SoF RNase H2 overexpression supports increased LINE-1 retrotransposition, despite reduced substrate affinity

We reasoned that overexpression of the RNase H2 SoF mutant may compensate for its reduced activity against RNA:DNA hybrids, and tested the effect of simultaneous overexpression of RNASEH2A-P40D/Y210A, RNASEH2B and RNASEH2C on LINE-1 retrotransposition. We found that overexpression of SoF RNase H2 indeed leads to increased LINE-1 retrotransposition compared to the β-arrestin control (Fig 6A, P = 0.019). To further investigate why the separation of function mutant failed to rescue retrotransposition in the complemented RNASEH2A-KO cells, whereas its overexpression did support a higher rate of retrotransposition, we compared enzyme kinetics for SoF and wildtype RNase H2 on RNA:DNA substrate (Fig EV4I). We established that the SoF mutant has much reduced substrate affinity (K_m^{SoF} ~ 16x K_m^{WT}), whereas its maximum substrate conversion rate is similar to that of WT RNase H2 (k_{cat}^{SoF} ~ 0.83x k_{cat}^{WT}). The reduced substrate affinity of SoF RNase H2 therefore provides a likely explanation for our observations. These findings are in keeping with a role for the activity of RNase H2 against RNA:DNA hybrids to support LINE-1 retrotransposition.

RNase H1 overexpression partially rescues LINE-1 retrotransposition in RNase H2 null cells

We assume RNase H1 to be expressed at normal levels in RNASEH2A-KO cells, and because of the marked reduction in LINE-1 retrotransposition in such null cells, it is unlikely that RNase H1 plays a major role in L1 retrotransposition. However, its activity against RNA:DNA hybrids may still contribute and could explain the variable level of remaining retrotransposition observed in our different RNase H2 null cells; retrotransposition was reduced between 4- and 15-fold compared to parental cells, depending on the cell line used. We therefore tested the effect of complementing HeLa RNASEH2A-KO cells with RNase H1. Two independent HeLa RNASEH2A-KO clones (KO1 and KO2) were transduced with a retroviral vector expressing the nuclear isoform of human RNase H1. To confirm overexpression of RNase H1, activity against RNA:DNA heteroduplexes was measured in lysates of these cells, showing a small but significant increase in enzyme activity (Fig 6B and Appendix Fig S4); RNASEH2A-KO1 cells complemented with wildtype RNase H1 displayed a 1.6-fold increase, while RNASEH2A-KO2 displayed a 2.2-fold increase in cleavage of RNA:DNA heteroduplexes, when compared to the corresponding EV complemented cells. As expected, no effect on RNase H activity against single embedded ribonucleotides was observed in the RNase H1 complemented cells (Fig 6C).

Next, we performed L1 retrotransposition assays using vector JJ101/L1.3, with RNASEH2A-complemented cells as positive controls. Notably, RNase H1 complementation partially alleviated the L1 retrotransposition defect seen in the parental RNASEH2A-KO clones, but not to the same extent as RNASEH2A complementation (3.4-fold increase for RNASEH2A vs 2.2-fold increase for RNase H1 compared to parental KO1; 2.5-fold vs 1.8-fold increase respectively for KO2, Fig 6D, E). Controls revealed that similar numbers of blasticidin-resistant colonies were formed for all cell lines when transfected with the control plasmid pcDNA6.1 (Fig 6D). Due to the relatively low increase in cellular RNase H activity against RNA:DNA heteroduplexes, failure to fully rescue retrotransposition is perhaps not surprising. However, the ability of RNase H1 to partially rescue L1 activity is consistent with the possibility that both cellular RNase H enzymes could facilitate L1 retrotransposition, and would be in line with a model in which these nucleases degrade the RNA:cDNA hybrid formed during TPRT. We therefore propose that RNase H2 facilitates LINE-1 retrotransposition by removing LINE-1 RNA after reverse transcription, allowing completion of the LINE-1 insertion event, with a minor contribution from nuclear RNase H1 (Fig 6F).

Reduced LINE-1 retrotransposition due to RNase H2 disease mutations

Overall, our data suggest that LINE-1 retrotransposition is likely to be reduced in cells from AGS patients with RNase H2 mutations, as most of these are known to cause reduced cellular enzyme activity. We confirmed the impact of disease mutations in any of the three subunits using recombinant RNase H2, but did not find the same change in cleavage pattern observed for the separation of function mutant (Fig EV5A, B). We speculate that the altered cleavage pattern for the latter may be due to its reduced substrate affinity, an effect that may be more pronounced closer to the substrate 3' end. To determine the cellular effect of RNase H2 disease mutations, we complemented RNASEH2A-KO cells with RNASEH2A-G37S and RNASEH2A-E225G, the only two missense mutations that have been found so far as causative homozygous changes in the catalytic subunit in AGS patients (Rice et al, 2013). Western-blot analyses revealed that these cells express mutant RNASEH2A (Fig 7A), leading to a small, but significant increase in cellular RNase H2 activity (Fig 7B). Notably, we observed partial rescue of LINE-1 retrotransposition in cells complemented with RNASEH2A-G37S and RNASEH2A-E225G (Fig 7C, D). Importantly, both AGS mutants displayed significantly reduced retrotransposition compared to RNASEH2A-WT complemented cells (n = 3, P = 0.003 for G37S, and P = 0.018 for E225G). Therefore, based on our data, we would expect AGS patients with RNase H2 mutations to have reduced levels of productive LINE-1 retrotransposition.

Discussion

RNase H2 has been suggested to control LINE-1 retrotransposition (Volkman & Stetson, 2014), similar to other AGS genes. While our work was under revision, Choi et al published work that suggests that RNase H2 may indeed act as a LINE-1 restriction factor (Choi et al, 2018). However, contrary to these findings, our results, using multiple independent CRISPR/Cas9 edited RNase H2 null clones, three different cell lines and several engineered LINE retrotransposition reporters, provide comprehensive evidence to support a role for cellular RNase H2 activity in promoting LINE-1 retrotransposition. Furthermore, our findings are consistent with a recent report that also found RNase H2 to be required for retrotransposition (Bartsch et al, 2017). We also demonstrate that other retrotransposons lacking an RNase H domain also rely on cellular RNase H activity to mobilise. In contrast, retrotransposons that code for an RNase H domain/activity did not require cellular RNase H2 to retrotranspose efficiently. Complementation of the retrotransposition defect in RNase H2 null cells by RNase H1 overexpression, and increased retrotransposition upon overexpression of the RNase H2 separation of function mutant lead us to propose a model in which RNase H2 degrades LINE-1 RNA in the RNA:cDNA retrotransposition intermediate generated during TPRT (Fig 6F).

Recently, a PCNA-Interaction-Protein (PIP) motif was identified in L1-ORF2p (Taylor et al, 2013), and the interaction between L1-ORF2p and PCNA was shown to be required for efficient retrotransposition. As RNASEH2B also contains a functional PIP domain that allows RNase H2 to interact with PCNA (Bubeck et al, 2011; Chon et al, 2009) we speculate that PCNA might act as an anchor protein connecting L1-ORF2p with RNase H2 during retrotransposition. This may also explain why RNase H1, which lacks a PIP domain, cannot efficiently complement the L1-retrotransposition defect inherent to RNase H2 null cells. However, nuclear RNase H1 could process LINE-1 RNA:cDNA hybrids by a simple but less efficient diffusion mechanism. Whether the interaction between PCNA and RNase H2 indeed contributes to efficient retrotransposition remains to be determined.

Our model, in which cellular RNase H activity promotes completion of LINE-1 retrotransposition by degrading the RNA from RNA:cDNA hybrids generated during TPRT (Fig 6F), would explain how LINE-1 elements can function without an active RNase H domain (Malik et al, 1999; Olivares et al, 2002). We provided several lines of evidence supporting this model: i) strongly reduced LINE-1 retrotransposition in RNase H2 null cells; ii) rescue of this defect by wildtype RNASEH2A as well as iii) RNase H1 overexpression; and iv) increased retrotransposition upon overexpression of both wildtype and separation

of function RNase H2. Our work shows that RNase H activity directed against RNA:DNA hybrids, mainly provided by cellular RNase H2, is important for efficient and productive LINE-1 retrotransposition. We interpret this to mean that it is involved in degrading LINE-1 RNA in the RNA:cDNA hybrid, allowing second strand synthesis and ultimately insertion into the genome. Alternative explanations are of course possible. As there is increasing evidence that DNA double strand break repair can be mediated by RNA (Keskin et al, 2014; Michelini et al, 2017; Ohle et al, 2016), one intriguing possibility is that RNA:DNA hybrids play a more active role in the LINE-1 retrotransposition process, for example by recruiting RNase H2 and DNA repair machinery. Furthermore, RNase H2 deficiency can also cause larger genomic rearrangements (Reijns et al, 2012) which might impact on LINE-1 retrotransposition. Although we cannot rule out that this type of genome instability interferes with retrotransposition, or even that non-productive retrotransposition contributes to increased genomic rearrangements in RNase H2 null cells, it seems unlikely that this is the reason for the reduced LINE-1 retrotransposition we observe, particularly as RNase H2 overexpression leads to increased rates of retrotransposition.

As mutations in the genes encoding RNase H2 are a frequent cause of AGS, our findings are relevant with regards to possible sources of immunostimulatory nucleic acids thought to cause autoinflammation. Two sources for such cytoplasmic nucleic acids have been proposed: DNA damage or retroelements. Notably, active LINE-1s are expressed and highly active in the central nervous system (Coufal et al, 2009; Muotri et al, 2005) and strong experimental evidence suggest that TREX1, SAMHD1 and ADAR1 act as LINE-1 restriction factors (Orecchini et al, 2017; Stetson et al, 2008; Thomas et al, 2017; Zhao et al, 2013). Although one study failed to detect elevated retrotransposition of L1s in the hippocampus of an AGS patient with SAMHD1 mutations (Upton et al, 2015), more recent work using TREX1-deficient neural cells generated from human embryonic stem cells has strongly implicated accumulating LINE-1 derived single-stranded DNAs (ssDNAs) in type I IFN production and neurotoxicity (Thomas et al, 2017), consistent with a role for active LINE-1s in AGS pathophysiology (Garcia Perez & Alarcon-Riquelme, 2017). This work also reinforces the concept that byproducts of active retrotransposition, rather than the accumulation of LINE-1 insertions per se, may be the driver of AGS pathology (Upton et al, 2015), with TREX1 normally degrading LINE-1 ssDNA retrotransposition intermediates (Garcia Perez & Alarcon-Riquelme, 2017; Stetson et al, 2008; Thomas et al, 2017).

Very recently, we have demonstrated both increased DNA damage and cGAS-STING dependent upregulation of interferon-stimulated genes (ISG) in RNase H2 null MEFs (Mackenzie et al, 2016). Furthermore, we established a mechanism linking genome instability to inflammation, with micronuclei providing a source of cytoplasmic DNA able to

activate cGAS, (Mackenzie et al, 2017), although the direct relevance of this to AGS remains to be determined. Notably, neither DNA damage nor the ISG response was alleviated by overexpression of RNase H1 (Mackenzie et al, 2016), in contrast to partial rescue of the retrotransposition defect in RNase H2 null HeLa cells overexpressing RNase H1 (Fig 6). We therefore favour the possibility that genome stability is the underlying cause of autoinflammation in AGS associated with RNase H2 mutations. However, because RNase H2 activity is required for LINE-1 retrotransposition and we show that cells with RNase H2 disease mutations have reduced levels of productive retrotransposition, it is formally possible that accumulation of nuclear LINE-1 RNA:cDNA hybrids is a source of immunostimulatory nucleic acids. How such hybrids that are covalently linked to the genome would access the cytoplasm and activate pattern recognition receptors is currently unclear though. An additional remaining question is whether physiological levels of retrotransposition byproducts are sufficient to elicit the observed inflammatory response. Clearly, further work is therefore needed to determine the relative importance of retroelement activity and genome instability in AGS. This will not be straight forward, as the two are not necessarily mutually exclusive.

In summary, our work contributes to the mechanistic understanding of LINE-1 retrotransposition, as we demonstrate that cellular RNase H2 plays an integral part in LINE retrotransposition, explaining how LINE elements lacking an RNase H domain can retrotranspose. In addition, our data adds a new layer of complexity to the understanding of AGS pathophysiology, as we demonstrate that not all AGS proteins are LINE restriction factors.

Material and Methods
Cell culture

HeLa cells, a kind gift from G. Stewart (Birmingham) originally obtained from ATCC, were grown in Dulbecco's Modified Eagle Medium (DMEM; Gibco, Cat no 41965-039) supplemented with 10% fetal bovine serum (FBS), 50 U/ml penicillin and 50 μg/ml streptomycin. U2OS cells purchased from the European Collection of Authenticated Cell Cultures (ECACC, Cat no. 92022711) and HCT116 p53$^{-/-}$ cells (Bunz et al, 1998; Dornan et al, 2004), a kind gift from K. Ball (Edinburgh), were maintained in modified McCoy's 5A medium (Gibco; Cat no 26600-023) supplemented with 10% FBS, 50 U/ml penicillin and 50 μg/ml streptomycin.

All cell lines were grown at 37°C, 5% CO_2 and atmospheric O_2, and passaged using Trypsin (Gibco). Checks were performed at least once a month using the Lonza-Mycoalert Mycoplasma Detection Kit to ensure that all cells were mycoplasma-free. In addition, the identity of the cell lines was confirmed by SRT analyses at least once a year (Lorgen, Granada, Spain).

Plasmid DNA

All plasmids were purified using a Plasmid Midi kit from Qiagen. DNA was analysed by electrophoresis (0.7% agarose-ethidium bromide gels) and only highly supercoiled DNA preparations were used in transfection experiments. Cloning strategies are available upon request.

pSpCas9n(RNASEH2A-g1)-2A-GFP and ***pSpCas9n(RNASEH2A-g2)-2A-Puro*** express guide RNAs (gRNAs) designed against exon 1 (TGCCCGCCTCATCGACGCCC) and intron 1 (CCCGTGCTGGGTGCGCCCCT) of human RNASEH2A, and Cas9n (D10A nickase mutant) fused to the cDNA of Enhanced Green Fluorescent Protein (EGFP) and puromycin N-acetyl-transferase (puro) respectively. gRNAs were generated by annealing DNA oligonucleotides and were cloned into the BbsI site of pSpCas9n(BB)-2A-GFP and pSpCas9n(BB)-2A-Puro vectors (Addgene plasmids #48140 and #48141, respectively; gifts from Feng Zhang) as previously described (Ran et al, 2013).

pMSCVpuro-RNASEH2A-WT, coding sequence of human RNASEH2A (NM_006397.2) cloned into vector pMSCVpuro-Dest, a Gateway compatible version of pMSCVpuro (Clontech).

pMSCVpuro-RNASEH2A-SoF, a derivative of plasmid pMSCVpuro-RNASEH2A-WT that contains two missense mutations in the coding sequence of human RNASEH2A (P40D/Y210A, separation of function mutant (Chon et al, 2013)).

pMSCVpuro-RNASEH2A-CD, a derivative of plasmid pMSCVpuro-RNASEH2A-WT that contains two missense mutations in the coding sequence of human RNASEH2A (D34A/D169A, catalytically inactive (Reijns et al, 2011)).

pMSCVpuro-RNaseH1, coding sequence of the nuclear isoform of the human RNASEH1 gene (NM_002936.5, aa27-286) cloned into pMSCVpuro-Dest.

pcDNA3.1/nV5-RNASEH2A, coding sequence of human RNASEH2A cloned into vector pcDNA3.1/nV5-DEST (contains an N-terminal V5 tag).

pcDNA3.1/nV5-RNASEH2A-SoF, coding sequence of human RNASEH2A with P40D/Y210A missense mutations cloned in vector pcDNA3.1/nV5-DEST (contains an N-terminal V5 tag).

pcDNA3.1/nV5-RNASEH2B, coding sequence of human RNASEH2B (NM_024570.3) cloned into pcDNA3.1/nV5-DEST (contains an N-terminal V5 tag).

pcDNA3.1/nV5-RNASEH2C, contains the coding sequence of the human RNASEH2C gene (NM_032193.3) cloned in pcDNA3.1/nV5-DEST (contains an N-terminal V5 tag).

pK-βarr, described previously (Bogerd et al, 2006) and expresses C-terminally HA-tagged human β-Arrestin.

pK-A3A, described previously (Bogerd et al, 2006) and expresses C-terminally HA-tagged human APOBEC3A.

pU6ineo, described previously (Richardson et al, 2014). Contains the neomycin phosphotransferase (NEO) expression cassette from pEGFP-N1 (Clontech) cloned into a modified pBSKS-II(+) (Stratagene) that contains a U6 promoter in the multi-cloning site.

pcDNA6.1, (Invitrogen) contains an expression cassette for blasticidin-S deaminase.

JM101/L1.3, described previously (Sassaman et al, 1997) and contains a full-length copy of the human L1.3 element tagged with the *mneoI* indicator cassette (Freeman et al, 1994; Moran et al, 1996) and is cloned in pCEP4 (Life Technologies).

JM101/L1.3-D205A, described previously (Wei et al, 2001); a derivative of JM101/L1.3 that contains a missense mutation in the EN domain of L1-ORF2p (D205A).

JM101/L1.3-D702A, was described previously (Wei et al, 2001); a derivative of JM101/L1.3 that contains a missense mutation in the RT domain of L1-ORF2p (D702A).

JJ101/L1.3, described previously (Kopera et al, 2011). It contains a full-length copy of the human L1.3 element (Sassaman et al, 1997) tagged with the *mblastI* indicator cassette (Goodier et al, 2007; Morrish et al, 2002) and is cloned in pCEP4 (Life Technologies).

JJ101/L1.3-D205A, described previously (Kopera et al, 2011); a derivative of JJ101/L1.3 that contains a missense mutation in the EN domain of L1-ORF2p (D205A).

JJ101/L1.3-D702A, described previously (Kopera et al, 2011); a derivative of JJ101/L1.3 that contains a missense mutation in the RT domain of L1-ORF2p (D702A).

pXY014, described previously (Xie et al, 2011); contains a full-length copy of the human L1RP element (Kimberland et al, 1999) tagged with the mflucI indicator cassette (Xie et al, 2011) and is cloned in a modified pCEP4 (Life Technologies) that contains a Renilla firefly expression cassette.

pXY017, described previously (Xie et al, 2011); a derivative of pXY014 that contains two missense mutations in the RNA binding domain of L1-ORF1p (RR261/62AA). This plasmid was used as a negative control of the luciferase-based retrotransposition assays.

pCMVMusD-6neo^{TNF}, described previously (Ribet et al, 2004); contains a full-length copy of a mouse MusD element (AC124426, positions 9078–16,569 (+)) tagged with the neo^{TNF} indicator cassette (Esnault et al, 2002) and is cloned in vector pCMVbeta (Clontech).

Zfl2-2mneoI, described previously (Garcia-Perez et al, 2010; Sugano et al, 2006); contains a full-length copy of the zebrafish Zfl2-2 element tagged with the *mneoI* indicator cassette inside the 3′UTR of the LINE (Freeman et al, 1994; Sugano et al, 2006) and is cloned in pCEP4 (Life Technologies).

pT2neo, described previously (Mates et al, 2009); contains an SV40-driven neomycin phosphotransferase cDNA flanked by SB TIRs.

pCMV-SB100x, described previously (Mates et al, 2009); contains a CMV-driven hyperactive SB Transposase.

pCEP-EGFP, described previously (Alisch et al, 2006); contains the coding sequence of the humanized EGFP protein cloned in pCEP4 (Invitrogen).

pGEX6P1-hsRNASEH2BCA, pGEX6P1-hsRNASEH2BCA(D34A/D169A), pGEX6P1-hsRNASEH2B(A177T)CA and ***pGEX6P1-hsRNASEH2BC(R69W)A***, described previously (Reijns et al, 2011) allow expression in *E. coli* of GST-tagged human RNASEH2B and non-tagged RNASEH2C and A subunits. Amino acid substitutions indicated in brackets were introduced into the relevant subunits by site-directed mutagenesis.

pGEX6P1-hsRNASEH2BCA(P40D/Y210A),   pGEX6P1-hsRNASEH2BCA(G37S) and *pGEX6P1-hsRNASEH2BCA(E225G)* had the P40D/Y210A separation of function mutations, and G37S and E225G AGS mutations respectively introduced into RNASEH2A by site-directed mutagenesis.

Generation of RNASEH2A knockout cell lines

To establish RNASEH2A-KO cell lines, cells were seeded in 6-well plates and transfected with the two vectors encoding both the sgRNAs and Cas9n using Lipofectamine 2000 (Thermo Fisher Scientific). Forty-eight hours after transfection, single EGFP-expressing cells were sorted into 96-well plates on a BD FACSJazz instrument (BD Biosciences) and grown until cell lines formed. RNASEH2A-KO clones were selected on the basis of the size of PCR products of the targeted region, and deletions/insertions subsequently confirmed by Sanger DNA sequencing. Oligonucleotides (5' to 3') used for PCR amplification and sequencing of targeted RNASEH2A loci were 5´-ACCCGCTCCTGCAGTATTAG and 5´-TCCCTTGGTGCAGTGCAATC. The absence of functional RNASEH2A was confirmed by immunoblotting, by an RNase H2 activity assay, and using alkaline gel electrophoresis as described below. Only clones confirmed to be functionally null were used for subsequent experiments. Some knockout clones retained very low levels of RNASEH2A protein expression, apparent upon long exposure of immunoblots. For these clones, Sanger sequencing showed the presence of in-frame deletions, in each case removing essential catalytic site residues, including Asp34, rendering them enzymatically non-functional. Clones expressing wild-type RNASEH2A protein were identified in parallel and used as controls.

Retroviral complementation

To complement RNASEH2A-KO HeLa clones, cells were infected with retroviral supernatant produced in Amphotropic Phoenix packaging cells (Swift et al, 2001) using pMSCVpuro-based vectors, in the presence of 4 µg/ml polybrene and selected for stable integration using 2 µg/ml puromycin.

Whole Cell extracts preparation and western blot analysis

Whole cell extracts (WCE) for RNase H activity assays and for determining protein levels of RNase H2 subunits were prepared by incubating cells in lysis buffer (50 mM Tris-HCl pH 8.0, 280 mM NaCl, 0.5% NP-40, 0.2 mM EDTA, 0.2 mM EGTA, 10% glycerol (vol/vol), 1

mM DTT and 1 mM phenylmethyl-sulfonyl fluoride (PMSF)) for 10 min on ice, followed by the addition of an equal volume of 20 mM HEPES pH 7.9, 10 mM KCl, 1 mM EDTA, 10% glycerol (vol/vol), 1 mM DTT and 1 mM PMSF for an additional 10 min. Whole cell extracts were cleared by centrifugation (17,000 g for 10 min at 4°C) and protein concentration was determined by Bradford assay (Protein Assay Kit, BioRad).

In overexpression assays conducted with HeLa and U2OS cells, WCEs were prepared using RIPA buffer (Sigma) supplemented with 1x Complete Mini EDTA-free Protease Inhibitor cocktail (Roche), 0.1% Phosphatase Inhibitor 1&2 (Sigma), 1mM (PMSF) (Sigma) and 0.25% β-mercaptoethanol (Sigma), incubating cells for 10 min on ice. Cellular debris was removed by centrifugation (1,000 g for 5 min at 4°C) and total protein concentration was determined using the Micro BCA Protein Assay Kit (Thermo) following standard procedures.

Equal amounts of protein lysates were run on SDS-PAGE gels and transferred to PVDF or nitrocellulose membranes (Bio-Rad). Membranes were blocked in 5% milk / TBST (TBS + 0.2% Tween-20 (v/v)) and incubated with primary antibodies diluted in 5% milk/TBST overnight at 4˚C. Membranes were then washed 3 times with TBST, incubated with secondary antibodies for 1 h at RT, washed again and developed. As secondary antibodies, we used Horseradish Peroxidase (HRP)-linked Antibodies (Cell Signaling) and either Amersham ECL Prime Western Blotting Detection Reagent (GE Healthcare Life Sciences) or an Inmun-StarTM Western CTM Detection Kit (BIO-RAD). The light signal was captured on X-ray films or using an ImageQuantLAS4000 device following manufacturer's recommendations. To quantify L1-ORF1p expression levels, we used an infrared fluorescent detection system (Odyssey, LI-COR) following manufacturer's recommendations.

The following antibodies were used for immunoblotting (at indicated dilutions): sheep anti-RNase H2 (raised against human recombinant RNase H2 (Reijns et al, 2012), 1:1,000); rabbit anti-RNASEH2A (Origene TA306706, 1:1,000) or mouse anti-RNASEH2A (Santa Cruz sc-515475, 1:1,000); mouse anti-α-tubulin B512 (Sigma T6074, 1:5,000); mouse anti-vinculin (Sigma V9264, 1:1,000); rabbit anti-L1Hs-ORF1p (provided by Dr Oliver Weichenrieder, Max-Planck, Germany, (Macia et al, 2017) 1:5,000); mouse anti–β-actin (1:20,000; Sigma); mouse anti-V5 (clone V5-10, Sigma V8012, 1:10,000). In quantitative westerns, goat anti-rabbit and anti-mouse fluorescent secondary antibodies were used at a 1:20,000 dilution.

RNase H2 activity assay

To assess RNase H2 activity in whole cell extracts, a FRET-based fluorescent substrate release assay was performed as previously described (Reijns et al, 2011). Briefly, RNase H2-specific activity was determined by measuring cleavage of a single embedded ribonucleotide containing double stranded DNA substrate (DRD:DNA). Activity against a DNA:DNA substrate of the same sequence was used to correct for non-RNase H2 "background activity" against the DRD:DNA substrate. Substrates were formed by annealing a 3'-fluorescein-labelled oligonucleotide (5′GATCTGAGCCTGGGaGCT or 5′GATCTGAGCCTGGGAGCT; uppercase DNA, lowercase RNA) to a complementary 5′ DABCYL-labelled DNA oligonucleotide (Eurogentec). Reactions were performed in 100 µl of reaction buffer (60 mM KCl, 50 mM Tris-HCl pH 8.0, 10 mM MgCl2, 0.01% BSA, 0.01% Triton X-100) with 250 nM substrate in 96-well flat-bottomed plates at 24°C. Whole cell lysates were prepared as described above, and the final protein concentration used per reaction was 100 ng/µl. Fluorescence was read (100 ms) every 5 min for up to 90 min using a VICTOR2 1420 multilabel counter (Perkin Elmer), with a 480-nm excitation filter and a 535-nm emission filter.

To assess RNase H2 activity in whole cell extracts using the gel-based assay, a range of protein concentrations (50 – 400 ng/µl) was incubated with 2 µM substrate (described above; 5′gatctgagcctgggagct for RNA:DNA) in 5 µl reactions at 37°C for 30 min or 1 h. Reactions were stopped through addition of an equal volume of 96% formamide, 20 mM EDTA, and heating at 95°C. Products were resolved by denaturing PAGE (20%, 1x TBE), visualized on a FLA-5100 imaging system (Fujifilm) and quantified using ImageQuant TL (GE Healthcare).

Detection of Ribonucleotides in Genomic DNA

Total nucleic acids were isolated from ~1 million cells by lysis in ice-cold buffer (20 mM Tris-HCl pH 7.5, 75 mM NaCl, 50 mM EDTA) and subsequent incubation with 200 µg/ml proteinase K (Roche) for 10 min on ice followed by addition of N-Lauroylsarcosine sodium salt (Sigma) to a final concentration of 1%. Nucleic acids were sequentially extracted with TE-equilibrated phenol, phenol:chloroform:isoamyl alcohol (25:24:1) and chloroform, then precipitated with isopropanol, washed with 75% ethanol and dissolved in nuclease-free water.

For alkaline gel electrophoresis, 500 ng of total nucleic acids were incubated with 1 pmol of purified recombinant human RNase H2 (Reijns et al, 2011) and 0.25 µg of DNase-free RNase (Roche) for 30 min at 37°C in 100 µl reaction buffer (60 mM KCl, 50 mM Tris-HCl pH 8.0, 10 mM MgCl2, 0.01% BSA, 0.01% Triton X-100). Nucleic acids were ethanol

precipitated, dissolved in nuclease-free water and separated on 0.7% agarose in 50 mM NaOH, 1 mM EDTA. After electrophoresis, the gel was neutralised in 0.7 M Tris-HCl pH 8.0, 1.5 M NaCl and stained with SYBR Gold (Invitrogen). Imaging was performed on a FLA-5100 imaging system (Fujifilm), and densitometry plots generated using an AIDA Image Analyzer (Raytest).

Retrotransposition Assays

LINE-1 retrotransposition assays in RNASEH2A-KO and control clones carried out in HeLa (n = 12) and HCT116 p53$^{-/-}$ (n = 6) cells were done blindly; in addition, at least 3 independent experiments were conducted per assay. Retrotransposition assays were carried out as previously described (Heras et al, 2013; Wei et al, 2000). Briefly, cells were plated in 6-well dishes (for retrotransposition and toxicity assays, Corning); when indicated, cells were plated in 10-cm plates (for toxicity assays, Corning). For assays employing human LINE-1-based constructs (plasmid JM101/L1.3 and mutants, JJ101/L1.3 and mutants, and pXY014 and mutants), approximately 2x10^4 cells were plated per well in a 6-well dish; when employing zebrafish LINEs (plasmid Zfl2-2$mneoI$) and LTR-retrotransposons (plasmid pCMVMusD-6neo^{TNF}), approximately 4x10^4 cells were plated per well in a 6-well dish; in toxicity assays (plasmids pU6ineo or pcDNA6.1), approximately 1x10^4 cells were plated per well in a 6-well dish; in some toxicity assays, approximately 4x10^4 cells were plated in 10-cm plates. Eighteen hours after plating, DNA transfections were carried out using FuGene 6 transfection reagent (Promega) and Opti-MEM (Life Technologies) following the protocol provided by the manufacturer (for a six well plate: 3 µl of FuGene and 97 µl of Opti-MEM and 1 µg of DNA transfected; for a 10-cm plate: 12 µl of FuGene and 388 µl of Opti-MEM and 4 µg of DNA transfected). The day after transfection, media was replaced with fresh media. Luciferase-based retrotransposition assays were analysed 96 h post-transfection using the Dual-Glo® luciferase assay system (Promega) following the protocol provided by the manufacturer. When G418 selection was applied ($mneoI$ containing plasmids), cells were subjected to selection with 400 µg/ml G418 (Life Technologies) starting approximately 72 h post-transfection; when blasticidin S selection was applied ($mblastI$ containing plasmids), cells were subjected to selection with 5 µg/ml blasticidin S (Life Technologies) starting approximately 120 h post-transfection; G418 selection was conducted for 12 days, while blasticidin S selection was carried out for 7 days. After selection, antibiotic resistant colonies were fixed with 2% paraformaldehyde/0.4% glutaraldehyde, and stained with 0.1% crystal violet solution as described (Moran et al, 1996; Wei et al, 2000). In all experiments, a co-transfection with plasmid pCEP-EGFP was carried out in parallel to control for Transfection Efficiency (TE);

co-transfected cells were harvested 72h post-transfection and we used FACS to determine the percentage of EGFP-expressing cells. In the overexpression experiments, to control for toxicity and colony forming capacity, cells were transfected in parallel with the indicated toxicity vector (either pU6i-NEO or pcDNA6.1) and colony numbers used for additional normalization as described (Kopera et al, 2016). Selection, fixation, and staining were conducted as described above.

Transposition Assays

To assay SB transposition in HeLa and U2OS parental cells, and derived RNASEH2A-KO and control clones, approximately 1×10^5 cells were plated per well in a 6-well dish. Eighteen hours after plating, DNA transfections were carried out using FuGene 6 and Opti-MEM following the protocol provided by the manufacturer (see above). Cells were transfected with 1 µg of plasmid pT2neo or co-transfected with 1 µg of plasmid pT2neo and 0.5 µg of plasmid pCMV-SB100x per well. Seventy-two hours after transfection, cells were trypsinised and counted; next, 10% of the transfected cells were plated on a 10-cm plate and G418 selection started forty-eight hours later (using 400 µg/ml). G418 selection was conducted for 10 days, and G418-resistant colonies were fixed with 2% paraformaldehyde/0.4% glutaraldehyde, and stained with 0.1% crystal violet solution. As in retrotransposition experiments, a co-transfection with plasmid pCEP-EGFP was carried out in parallel to control for TE differences.

PCR-based mutation analyses

To test whether RNase H2 deficiency caused increased mutation rates in de novo inserted L1-sequences, we used a previously described assay (Bogerd et al, 2006). Briefly, parental HeLa, HeLa RNASEH2A-KO1 and KO2 cells were plated (1×10^5 cells per well in a 6-well dish) and 18 h later transfected with 1 µg of plasmid JM101/L1.3 or with plasmid JM101/L1.3-D702A as a control, using the conditions described above. Forty-eight (2 d) and one hundred and twenty hours (5 d) after transfection, genomic DNA (gDNA) was isolated from transfected cells, digested with *Swa*I (NEB; there is a single *Swa*I site within the intron of the *mneo*I retrotransposition indicator cassette) and used as template in PCR reactions using primers NEO437s (5'GAGCCCCTGATGCTCTTCGTCC) and NEO1808as (5' CATTGAACAAGATGGATTGCACGC), that flank the engineered intron in *mneo*I. PCR reactions were carried in 25 µl using KAPA Taq ReadyMIx PCR and 0.4 µM of each primer. DNA-free water (Gibco) was included as a negative control in all assays, as well as PCR reactions conducted on gDNA isolated from naïve HeLa, and gDNA from naïve HeLa

digested with *Swa*I. PCR conditions for NEO amplification were as follows: 1x (95ºC, 3 min); 40x (15s, 95ºC; 15s, 60ºC; 30s, 72ºC) 1x, (72ºC, 1 min). PCR products were resolved on 1.5% agarose gels, amplified products excised, purified, and cloned in pGEMT-Easy (Promega). We sequence 15-20 clones per sample using M13FWD primer.

Statistics

Unless otherwise stated, all statistics were performed using two-sided unpaired t-test (parametric) or Mann-Whitney test (non-parametric) comparing replicates as indicated. $P < 0.05$ was considered as statistically significant.

Acknowledgements

Author Contributions

M.B.-G. and C.L.-R. performed all retrotransposon-related experiments, with the help/advice of S.R.H., M.G.-C., R.V.-A., D.C. and L.S. M.A.M.R performed all RNase H biochemistry experiments. T.C.W. conducted the tandem repeat sequence analyses. All KO and complemented cell lines were generated and characterised by Z.T., O.M., M.M.M., A.F., M.J.H.C.K. and M.A.M.R.; S.R.H. and A.S.-P. provided valuable input throughout the project. M.A.M.R., A.P.J. and J.L.G.-P. directed and designed the study. J.L.G.-P. and M.A.M.R. wrote the manuscript, with input from all authors.

Conflict of Interest

None of the authors declare any Conflict of Interest.

Figure Legends

Figure 1. Reduced LINE-1 retrotransposition in RNase H2 null HeLa cells

A. Western blot analysis shows absence of RNASEH2A and reduced RNASEH2B and C in RNASEH2A-KO clones (KO1-6), compared to parental cells or control clones (C1-5). Tubulin was used as a loading control. See also Source Data.

B. RNase H assay shows absence of activity against single embedded ribonucleotides in KO clones, with a smaller, but consistent reduction in all control clones. Activity in parental HeLa cells set at 100%. Data points represent the mean of 3 technical replicates for individual clones. Lines indicate the mean of 6 biological replicates (C1-6 and KO1-6) ± SEM.

C. High levels of genome embedded ribonucleotides in KO clones. Genomic DNA isolated from parental cells, KO and control clones, was RNase H2 treated and separated by alkaline gel electrophoresis. Smaller fragments indicate larger numbers of embedded ribonucleotides.

D. Schematic of retrotransposition vector JJ101/L1.3 (see also Figure EV1A). Within L1-ORF2p, relative positions of EN (endonuclease), RT (Reverse Transcriptase) and C (cysteine-rich) domains are indicated. Orange box with backward BLAST label depicts the retrotransposition indicator cassette *mblastl*.

E. Quantification of L1-WT retrotransposition, normalised to the level in parental cells and normalised for transfection efficiency (TE), set to 100% for comparison. Data points represent the mean of 3 technical replicates for individual clones. Lines indicate the mean of 6 biological replicates (C1-6 and KO1-6) ± SEM (representative of 6 independent experiments). Mann Whitney test; **, $P < 0.001$

F. Representative retrotransposition assay conducted in parental cells, control clones (C1-6), and RNASEH2A-KO clones (KO1-6). Cells were transfected with JJ101/L1.3 vectors containing an active human LINE-1 (WT-hL1, element L1.3), an EN-mutant LINE-1 (ENm-hL1, L1.3 D205A) or an RT-mutant LINE-1 (RTm-hL1, L1.3 D702A).

Figure 2. Reduced LINE-1 retrotransposition in RNase H2 null U2OS cells

A. Western blot analysis shows absence of RNASEH2A and reduced RNASEH2B and C in RNASEH2A-KO clones (KO1, KO2), compared to parental cells or a control clone (C1). Vinculin was used as a loading control. See also Source data.

B. RNase H assay shows absence of activity against single embedded ribonucleotides in KO clones, compared to control cells. Activity in parental U2OS cells set at 100%. Mean ± SD for 2 independent experiments.

C. High levels of genome embedded ribonucleotides in U2OS RNASEH2-KO clones. Genomic DNA were isolated from parental cells, KO and control clones, RNase H2 treated and separated by alkaline gel electrophoresis. Smaller fragments indicate more genome embedded ribonucleotides.

D. Schematic of plasmid JJ101/L1.3 and representative retrotransposition and toxicity assays conducted in parental U2OS cells, a control clone (C1), and two RNASEH2A-KO clones (KO1 and KO2). Cells were transfected with vectors containing an active human LINE-1 (WT-hL1, element L1.3), an RT-mutant (RTm-hL1, L1.3 D702A), or a toxicity control vector (CTRL, pcDNA6.1). Quantification of L1-WT retrotransposition, with the level in parental cells set to 100% for comparison. Plotted, mean ± SD for 3 technical replicates. Indicated is the average of n = 2 controls (parental, C1) and n = 2 (KO1, KO2) ± SD (representative of 3 independent experiments).

Figure 3. RNase H2 activity is required for LINE activity but dispensable for LTR-retroelement and DNA-Transposon activity

A. Schematic of retrotransposition vectors Zfl2-2*mneoI* and JM101/L1.3. The relative position of the EN domain (endonuclease), RT domain (Reverse Transcriptase) and C domain (cysteine-rich), if present, is indicated. The purple box with a backward NEO label depicts the retrotransposition indicator cassette *mneoI*.

B. Representative retrotransposition assays conducted in parental cells, control (C2), and RNASEH2A-KO (KO2) clones. Cells were transfected with vectors containing an active human LINE-1 (WT-hL1, element L1.3), an RT-mutant human LINE-1 (RTm-hL1, L1.3 D702A), or an active zebrafish LINE-2 (WT-zL2, element Zfl2-2).

C. Quantification of WT-hL1 (circles) and WT-zL2 (squares) retrotransposition in HeLa cells, normalised to the level in parental cells (set at 100%). Data points represent the mean of 3 technical replicates for individual clones. Lines indicate the mean of 5 biological replicates (C2-6 and KO2-6) ± SEM (representative of 3 independent experiments). For WT-hL1, in control lines (n = 5) retrotransposition levels averaged 83±2.5%; in null lines (n = 5) retrotransposition levels averaged 7±2.3%. Mann Whitney test; **, P < 0.001.

D. Left, schematic of a neo[TNF] tagged MusD LTR-retrotransposon. The relative position of the gag, pro and pol genes is indicated. The purple box with a backward NEO label depicts

the retrotransposition indicator cassette neo[TNF]. Right, quantification of MusD retrotransposition, normalised to the level in parental cells (set at 100%). Data points represent the mean of 3 technical replicates for individual clones. Lines indicate the mean of 6 biological replicates (C1-6 and KO1-6) ± SEM (representative of 3 independent experiments). t- test; ns, $P > 0.05$.

E. Left, schematic of the two plasmids used in Sleeping Beauty transposition assays. The purple box with a NEO label depicts the neo expression cassette. Underneath, a representative result is shown for DNA-Transposition assays (pT2neo + SB100x) or controls (only pT2neo). Right, quantification of the SB transposition results (pT2neo + SB100x samples), with the level in parental cells set at 100% for comparison. Mean ± SD for n = 3 technical replicates (representative of 3 independent experiments).

Figure 4. RNase H2 overexpression increases LINE-1 retrotransposition in HeLa and U2OS cells

A, B. Panels (A) (HeLa cells) and (B) (U2OS cells) follow the same nomenclature. Shown is a representative result for retrotransposition and toxicity assays, underneath a schematic of the retrotransposition vector JJ101/L1.3 used. Cells were transfected with JJ101/L1.3 (as indicated: WT-hL1 (L1.3), active human LINE-1; ENm-hL1 (D205A), EN-mutant; RTm-hL1 (D702A), RT-mutant) or the toxicity control vector (CTRL, pcDNA 6.1), indicated in the top), alongside an expression vector for β-arrestin as a negative control (-ve), the three RNase H2 subunits (RNase H2, at a 1:1:1 ratio), or a plasmid expressing APOBEC3A as a positive control (+ve) known to restrict LINE-1 retrotransposition. Right panel, quantification of this retrotransposition assay; with the level in cells co-transfected with β-arrestin set at 100% for comparison. Values were normalised for transfection efficiency and toxicity. Mean ± SD for n = 3 technical replicates (representative of 4 independent experiments). Unpaired two-sided t-test; **, $P < 0.01$; ***, $P < 0.001$

Figure 5. Complementation of RNASEH2A-KO cells with wildtype, but not separation of function RNASEH2A rescues LINE-1 retrotransposition

A, B. RNase H activity assays against single embedded ribonucleotides using recombinant purified proteins (RNASEH2A-WT and RNASEH2A-SoF). Note that only RNASEH2A-WT shows activity in this assay. Plotted, mean ± SEM for 3 independent experiments.

C, D. RNase H activity assays against RNA:DNA heteroduplexes using recombinant purified proteins (RNASEH2A-WT and RNASEH2A-SoF). Note that the pattern of products

generated by RNASEH2A-SoF is different from the wildtype pattern. Plotted, mean ± SEM for 3 independent experiments.

E. Western blot analysis of RNase H2 expression in RNASEH2A-KO HeLa cells complemented with the indicated retroviral vector (EV, empty vector; WT, wildtype RNASEH2A; SoF, RNASEH2A-P40D/Y210A; CD, RNASEH2A-D34A/D169A, see main text for details). Tubulin was used as a loading control. See also Source Data.

F. RNase H activity against single embedded ribonucleotides in RNASEH2A-KO cells is only rescued by wildtype RNASEH2A (KO1+WT). DRD:DNA heteroduplex (18 bp; ribonucleotide-containing strand 3'-labelled) was incubated with increasing amounts of whole cell lysate from the indicated cell line, and separated by denaturing PAGE. The graph shows mean values ± SEM for 3 independent experiments.

G. RNase H activity against RNA:DNA heteroduplexes in RNASEH2A-KO cells is rescued by wildtype (KO1+WT), not by CD RNASEH2A (KO1+CD) or the empty vector (KO1+EV). Note reduced activity and the difference in cleavage pattern produced by SoF RNASEH2A (KO1+SoF). RNA:DNA heteroduplex (18 bp; RNA strand 3'-labelled) was incubated with increasing amounts of whole cell lysate from the indicated cell line, and separated by denaturing PAGE. Plotted, mean ± SEM for 3 independent experiments.

H. Only wildtype RNASEH2A rescues the LINE-1 retrotransposition defect in RNASEH2A-KO cells. Left, representative retrotransposition and toxicity assays conducted in the four complemented lines. Cells were transfected with vectors containing an active human LINE-1 (WT-hL1, L1.3), an RT-mutant LINE-1 (RTm-hL1, D702A), or a toxicity control plasmid (CTRL, pcDNA 6.1). Right, quantification of L1-WT retrotransposition. For comparison, the retrotransposition level in KO1 cells complemented with the empty vector (EV) was set at 100%. Mean ± SD for n = 3 technical replicates (representative of 6 independent experiments).

Figure 6. Cellular RNase H activity against RNA:DNA hybrids is important for L1 retrotransposition

A. Increased L1 retrotransposition upon RNase H2 SoF overexpression. Left, representative retrotransposition and toxicity assays. HeLa cells were transfected with vectors containing an active LINE-1 (WT-hL1, L1.3), alongside an expression vector for β-arrestin as a negative control (-ve), the three RNase H2 subunits (RNase H2, at a 1:1:1 ratio; with RNASEH2A-WT or SoF), or a plasmid expressing APOBEC3A as a positive control (+ve) known to restrict LINE-1 retrotransposition. Right panel, quantification of this

retrotransposition assay; with the level in cells co-transfected with β-arrestin set at 100% for comparison. Values were normalised for transfection efficiency and toxicity. Mean ± SD for *n* = 2 technical replicates (representative of 3 independent experiments). Unpaired two-sided t-test; *, *P* < 0.05.

B. RNase H activity against RNA:DNA heteroduplexes in RNASEH2A-KO cells (clones KO1 and KO2) is partially rescued by overexpression of human nuclear RNase H1 (KO1+H1 and KO2+H1 vs KO1+EV and KO2+EV). RNA:DNA heteroduplex (18 bp; RNA strand 3'-labelled) were incubated with whole cell lysate and speed of cleavage determined using a FRET-based assay. Mean values ± SEM for *n* = 6 independent experiments.

C. RNase H activity against single embedded ribonucleotides in RNASEH2A-KO cells (clones KO1 and KO2) is not rescued by human RNase H1 (KO1+H1 and KO2+H1 vs KO1+EV and KO2+EV). Speed of cleavage of an 18 bp substrate was determined using a FRET-based assay. Mean values ± SEM for *n* = 3 independent experiments.

D, E. Representative retrotransposition and toxicity assays (D) conducted in the RNASEH2-KO clones (KO1 and KO2) complemented with RNASEH2A-WT (+RNASEH2A) or with human RNase H1 (+RNASEH1). Cells were transfected with vectors containing an active LINE-1 (WT-hL1, L1.3), an RT-mutant LINE-1 (RTm-hL1, D702A), or a toxicity control plasmid (CTRL, pcDNA6.1). Quantification of L1-WT retrotransposition (E). For comparison, the retrotransposition level in KO1 or KO2 cells was set at 100%. Mean ± SD for *n* = 3 technical replicates (representative of 3 independent experiments). Unpaired two-sided t-test; **, *P* < 0.01; ***, *P* < 0.001

F. Model for the initial steps of LINE-1 retrotransposition. For details, see main text.

Figure 7. Reduced L1 retrotransposition due to RNase H2 AGS mutations

A. Western blot analysis of RNase H2 expression in RNASEH2A-KO HeLa cells (KO2) complemented with the indicated retroviral vector (EV, empty vector; WT, wildtype RNASEH2A; RNASEH2A-G37S; RNASEH2A-E225G). Actin was used as a loading control. See also Source Data.

B. Complementation of RNASEH2A-KO cells with RNASEH2A with AGS mutations (G37S and E225G) leads to a small but significant increase in RNase H activity. Mean values ± SEM for *n* = 3 independent experiments. Unpaired two-sided t-test; *, *P* < 0.05; ns, *P* > 0.05.

C, D. Cells expressing AGS mutant RNase H2 fail to support efficient L1 retrotransposition. (C) Representative retrotransposition and toxicity assays conducted in the four

complemented lines. Cells were transfected with vectors containing an active human LINE-1 (WT-hL1, L1.3), an RT-mutant LINE-1 (RTm-hL1, D702A), or a toxicity control plasmid (CTRL, pcDNA 6.1). (D) Quantification of L1-WT retrotransposition in the complemented lines. For comparison, the retrotransposition level in KO cells complemented with empty vector (EV) was set at 100%. Mean ± SD for n = 3 independent experiments (each experiment performed in technical duplicates). Unpaired two-sided t-test; *, P < 0.05; **, P < 0.01.

Figure EV1. Reduced LINE-1 retrotransposition in HeLa RNase H2 null cells

A. Rationale of the retrotransposition assay using *mblastI* tagged LINE-1s (orange box with a backward BLAST label). Schematic of the retrotransposition vector JJ101/L1.3. Within the *mblastI* cassette, the orange arrow and the orange lollipop indicate the presence of a promoter and polyadenylation signal respectively. Within L1-ORF2p, the relative position of the EN (endonuclease), RT (Reverse Transcriptase) and C (cysteine-rich) domains is indicated. SD and SA indicate splice donor and acceptor sites respectively. Upon transcription from the CMV promoter located upstream of the L1, the L1 mRNA can be spliced by canonical *cis*-splicing and undergo a round of retrotransposition, resulting in the activation of the *mblastI* reporter and subsequent translation of the blasticidin deaminase protein (orange oval with blue BLAST label). In the retrotransposition event shown, the black arrows indicate the presence of Target Site Duplications (TSDs) flanking the 5' truncated insertion.

B. Toxicity controls: similar numbers of blasticidin-resistant colonies were generated for all cell lines after transfection with the pcDNA6.1 control vector (schematic). Representative results of transfection/selection experiments in parental HeLa cells, control clones (C1-6) and KO clones (KO1-6) are shown.

C. Rationale and schematic of plasmid pYX014. With this plasmid, L1 retrotransposition activates Firefly luciferase expression. Briefly, an active human L1 is tagged with a luciferase retrotransposition indicator cassette (yellow box with a backward F-luc label). Note that the backbone of the plasmid contains an expression cassette for Renilla Luciferase, to normalise transfection (big white arrow with R-luc label). The black arrow and the black lollipop indicate the presence of a promoter and polyadenylation signal respectively in the F-luc cassette. Upon transfection of plasmid pXY014 in cells, transcription from the 5′-UTR of L1, the L1 mRNA can be spliced by canonical *cis*-splicing and undergo a round of retrotransposition, resulting in the activation of the firefly luciferase reporter and subsequent translation of the F-luciferase protein (yellow star with F-luc label). On the other hand, the R-luc cassette on the plasmid can be transcribed and translated

into renilla luciferase (white star with R-luc label). In the retrotransposition event shown, the black arrows indicate the presence of TSDs flanking the 5' truncated insertion.

D. Results from retrotransposition assays conducted in HeLa parental cells, 3 control clones (C), and 3 RNASEH2A-KO clones (KO). The retrotransposition level in parental cells was set at 100%. Dots represent the mean of 3 technical replicates for individual clones. Lines indicate the mean of 3 biological replicates (C2, 4 and 5, and KO2-4) ± SEM (representative of 3 independent experiments). t-test, ***, $P < 0.001$

E, F. Western blot analysis of L1-ORF1p expression (in triplicate) in parental HeLa cells, a control clone (C1) and two KO clonal lines (KO1 and KO2), shows no indirect effect of RNase H2 deficiency on L1 expression. Tubulin (**E**) or β-actin (**F**) was used as a loading control. See also Source Data.

G. Quantification of Western blot from panel (C) using a LICOR device following manufacturer's instructions.

Figure EV2. RNase H2 activity is required for productive LINE retrotransposition in HeLa and U2OS cells

A. Schematic of retrotransposition vectors Zfl2-2mneoI (zebrafish LINE-2) and JM101/L1.3 (Human L1.3). The relative position of the EN domain (endonuclease), RT domain (Reverse Transcriptase) and C domain (cysteine-rich), if present, is indicated. The purple box with a backward NEO label depicts the retrotransposition indicator cassette *mneoI.* Underneath, representative retrotransposition assays conducted in HeLa parental cells, control (C2-6), and RNASEH2A-KO (KO2-6) clones (used for quantifications in Figure 3C). Cells were transfected with an active human LINE-1 (WT-hL1, element L1.3), an RT-mutant human LINE-1 (RTm-hL1, D702A), or an active zebrafish LINE-2 (WT-zL2, element Zfl2-2) vector.

B. Representative retrotransposition and toxicity assays conducted in parental U2OS cells, a control clone (C1), and two RNASEH2A-KO clones (KO1 and KO2). Cells were transfected with an active human LINE-1 (WT-hL1, element L1.3), an RT-mutant human LINE-1 (RTm-hL1, D702A), or an active zebrafish LINE-2 (WT-zL2, element Zfl2-2) vector. Right, quantification of WT-hL1 (dark grey bars) and WT-zL2 (light grey bars) retrotransposition in U2OS cells, with retrotransposition in parental cells for both elements set at 100% for comparison. Mean ± SD for *n* = 3 technical replicates (representative of 3 independent experiments).

Figure EV3. RNase H2 overexpression facilitates L1 retrotransposition

A. Anti-V5 Western blots using lysates of HeLa (left) or U2OS (right) cells transfected with the indicated plasmids. Cells were transfected with each independent RNase H2 subunit (left side) or co-transfected with the three subunits using two different ratios (1:1:1 or 14:7:1). β-actin was used as loading control. Asterisks indicate the presence of individual subunits. See also Source Data.

B, C. Schematic of the retrotransposition vector JJ101/L1.3. Underneath, representative results from retrotransposition and toxicity assays conducted in HeLa (**B**) or U2OS (**C**) cells. Cells were transfected with vector JJ101/L1.3 or with the toxicity control vector (CTRL, pcDNA6.1) alongside an expression vector for β-arrestin (used as a negative control, -ve) or for each of the three RNase H2 subunits at the indicated ratio (RNase H2 14:7:1). Labels indicate if cells were transfected with an active human LINE-1 (WT-hL1, element L1.3), an EN-mutant LINE-1 (ENm-hL1, D205A), an RT-mutant LINE-1 (RTm-hL1, D702A), or with the toxicity control plasmid (CTRL, pcDNA6.1). Right panels, L1-WT retrotransposition quantifications, with the retrotransposition level in cells co-transfected with β-arrestin (-ve) set at 100% for comparison. Values were normalised for transfection efficiency and toxicity. Mean ± SD for *n* = 3 technical replicates (representative of 4 independent experiments). Unpaired two-sided t-test; *, $P < 0.05$

Figure EV4. Complementation of RNASEH2A-KO HeLa cells

A. Schematic of substrates used in RNase H activity assays. These assays either use an 18-bp RNA:DNA hybrid (left), or a short dsDNA containing a single embedded ribonucleotide (DRD:DNA). RNASEH2A-WT can cleave both with high efficiency (++++), whereas RNASEH2A-CD (with D34A and D169A mutations) cannot cleave either (-). The separation of function mutant (SoF, with P40D and Y210A mutations) retains some activity against RNA:DNA heteroduplexes (++), but has virtually no activity against single embedded ribonucleotides (-).

B. RNase H2 SoF has reduced activity against RNA:DNA heteroduplexes and does not fully process the hybrid, even at high concentration and/or long incubation times. RNase H activity was measured using the 18-bp RNA:DNA substrate, separating products by denaturing PAGE after cleavage with RNase H2. WT, SoF and CD RNase H2 were used at 0.25 nM for 4 h (left) or 2.0 nM for 2 h (right). Note, the different pattern of products generated for SoF and WT.

C. As expected, the high levels of genome embedded ribonucleotides in RNASEH2A-KO cells is rescued only by complementation with wildtype RNASEH2A (+WT), not by SoF RNASEH2A (+SoF), CD RNASEH2A-A (+CD) or the empty vector (+EV). Genomic DNA

was isolated from parental cells, a control clone (C1) and the four complemented cell lines (+EV, +WT, +SoF and +CD), RNase H2 treated and separated by alkaline gel electrophoresis. Smaller fragments indicate larger numbers of embedded ribonucleotides.

D-G. Representative gels (used for quantifications in Figure 5F and G) with results from RNase H activity against single embedded ribonucleotides (D and E) and activity against RNA:DNA heteroduplexes (F and G) assays conducted with lysates from the indicated cell lines. Because RNase H1 is expressed in all of these cells, activity measured against RNA:DNA heteroduplex substrate in RNASEH2A-KO cell lysates is not completely absent. In addition, it is likely that other nucleases present in the cell lysate act (non-specifically) on the substrate, causing further background activity on both substrates.

H. Wildtype RNASEH2A rescues the LINE-1 retrotransposition defect in RNASEH2A-KO2 cells. Representative retrotransposition and toxicity assays conducted in RNASEH2A-KO2 cells and RNASEH2A-KO2 complemented with wildtype RNASEH2A (+WT). Cells were transfected with an active human LINE-1 (WT-hL1, element L1.3), an RT-mutant LINE-1 (RTm-hL1, D702A), or a toxicity control plasmid (CTRL, pcDNA6.1). Right panel, quantification of L1-WT retrotransposition. For comparison, the retrotransposition level in KO2 cells was set at 100%. Mean ± SD for n = 3 technical replicates (representative of 3 independent experiments).

I. RNase H2 SoF has reduced RNA:DNA heteroduplex substrate affinity. Initial substrate conversion rates (V_i) by 0.1 nM recombinant RNase H2 were measured at different 18-mer RNA:DNA substrate concentrations. Mean ± SEM for n = 3 independent experiments. K_m and k_{cat} ± SEM were calculated in GraphPad Prism 5.04, using non-linear regression. Change for SoF compared to WT indicated between brackets.

Figure EV5. Reduced enzyme activity for recombinant RNase H2 carrying AGS disease mutations.

A, B. RNase H activity assays (against 18-mer RNA:DNA heteroduplex) using the indicated recombinant purified proteins. Wild type or mutant recombinant RNase H2 (RNASEH2A-P40D/Y210A, RNASEH2A-G37S, RNASEH2A-E225G, RNASEH2B-A177T and RNASEH2C-R69W) were tested using the indicated protein concentration. As previously shown (Reijns et al, 2011), the A177T mutation had limited impact on enzyme activity; whereas the G37S, E225G and R69W mutations all caused a substantial reduction in RNase H2 activity. Note that only RNase H2-SoF (RNASEH2A-P40D/Y210A) generates an altered cleavage pattern. Shown are representative results from 3 independent experiments.

References

Alisch RS, Garcia-Perez JL, Muotri AR, Gage FH, Moran JV (2006) Unconventional translation of mammalian LINE-1 retrotransposons. *Genes Dev* **20:** 210-224

Bartsch K, Knittler K, Borowski C, Rudnik S, Damme M, Aden K, Spehlmann ME, Frey N, Saftig P, Chalaris A, Rabe B (2017) Absence of RNase H2 triggers generation of immunogenic micronuclei removed by autophagy. *Hum Mol Genet* **26:** 3960-3972

Beck CR, Collier P, Macfarlane C, Malig M, Kidd JM, Eichler EE, Badge RM, Moran JV (2010) LINE-1 retrotransposition activity in human genomes. *Cell* **141:** 1159-1170

Bogerd HP, Wiegand HL, Hulme AE, Garcia-Perez JL, O'Shea KS, Moran JV, Cullen BR (2006) Cellular inhibitors of long interspersed element 1 and Alu retrotransposition. *Proc Natl Acad Sci U S A* **103:** 8780-8785

Brouha B, Schustak J, Badge RM, Lutz-Prigge S, Farley AH, Moran JV, Kazazian HH, Jr. (2003) Hot L1s account for the bulk of retrotransposition in the human population. *Proc Natl Acad Sci U S A* **100:** 5280-5285

Bubeck D, Reijns MA, Graham SC, Astell KR, Jones EY, Jackson AP (2011) PCNA directs type 2 RNase H activity on DNA replication and repair substrates. *Nucleic Acids Res* **39:** 3652-3666

Bunz F, Dutriaux A, Lengauer C, Waldman T, Zhou S, Brown JP, Sedivy JM, Kinzler KW, Vogelstein B (1998) Requirement for p53 and p21 to sustain G2 arrest after DNA damage. *Science* **282:** 1497-1501

Cerritelli SM, Crouch RJ (2009) Ribonuclease H: the enzymes in eukaryotes. *The FEBS journal* **276:** 1494-1505

Cerritelli SM, Frolova EG, Feng C, Grinberg A, Love PE, Crouch RJ (2003) Failure to produce mitochondrial DNA results in embryonic lethality in Rnaseh1 null mice. *Mol Cell* **11:** 807-815

Choi J, Hwang SY, Ahn K (2018) Interplay between RNASEH2 and MOV10 controls LINE-1 retrotransposition. *Nucleic Acids Res* **46:** 1912-1926

Chon H, Sparks JL, Rychlik M, Nowotny M, Burgers PM, Crouch RJ, Cerritelli SM (2013) RNase H2 roles in genome integrity revealed by unlinking its activities. *Nucleic Acids Res* **41:** 3130-3143

Chon H, Vassilev A, DePamphilis ML, Zhao Y, Zhang J, Burgers PM, Crouch RJ, Cerritelli SM (2009) Contributions of the two accessory subunits, RNASEH2B and RNASEH2C, to the activity and properties of the human RNase H2 complex. *Nucleic Acids Res* **37:** 96-110

Clark AB, Lujan SA, Kissling GE, Kunkel TA (2011) Mismatch repair-independent tandem repeat sequence instability resulting from ribonucleotide incorporation by DNA polymerase epsilon. *DNA repair* **10:** 476-482

Cost GJ, Feng Q, Jacquier A, Boeke JD (2002) Human L1 element target-primed reverse transcription in vitro. *The EMBO journal* **21:** 5899-5910

Coufal NG, Garcia-Perez JL, Peng GE, Marchetto MC, Muotri AR, Mu Y, Carson CT, Macia A, Moran JV, Gage FH (2011) Ataxia telangiectasia mutated (ATM) modulates long

interspersed element-1 (L1) retrotransposition in human neural stem cells. *Proc Natl Acad Sci U S A* **108:** 20382-20387

Coufal NG, Garcia-Perez JL, Peng GE, Yeo GW, Mu Y, Lovci MT, Morell M, O'Shea KS, Moran JV, Gage FH (2009) L1 retrotransposition in human neural progenitor cells. *Nature* **460:** 1127-1131

Crow YJ, Chase DS, Lowenstein Schmidt J, Szynkiewicz M, Forte GM, Gornall HL, Oojageer A, Anderson B, Pizzino A, Helman G, Abdel-Hamid MS, Abdel-Salam GM, Ackroyd S, Aeby A, Agosta G, Albin C, Allon-Shalev S, Arellano M, Ariaudo G, Aswani V, Babul-Hirji R, Baildam EM, Bahi-Buisson N, Bailey KM, Barnerias C, Barth M, Battini R, Beresford MW, Bernard G, Bianchi M, Billette de Villemeur T, Blair EM, Bloom M, Burlina AB, Carpanelli ML, Carvalho DR, Castro-Gago M, Cavallini A, Cereda C, Chandler KE, Chitayat DA, Collins AE, Sierra Corcoles C, Cordeiro NJ, Crichiutti G, Dabydeen L, Dale RC, D'Arrigo S, De Goede CG, De Laet C, De Waele LM, Denzler I, Desguerre I, Devriendt K, Di Rocco M, Fahey MC, Fazzi E, Ferrie CD, Figueiredo A, Gener B, Goizet C, Gowrinathan NR, Gowrishankar K, Hanrahan D, Isidor B, Kara B, Khan N, King MD, Kirk EP, Kumar R, Lagae L, Landrieu P, Lauffer H, Laugel V, La Piana R, Lim MJ, Lin JP, Linnankivi T, Mackay MT, Marom DR, Marques Lourenco C, McKee SA, Moroni I, Morton JE, Moutard ML, Murray K, Nabbout R, Nampoothiri S, Nunez-Enamorado N, Oades PJ, Olivieri I, Ostergaard JR, Perez-Duenas B, Prendiville JS, Ramesh V, Rasmussen M, Regal L, Ricci F, Rio M, Rodriguez D, Roubertie A, Salvatici E, Segers KA, Sinha GP, Soler D, Spiegel R, Stodberg TI, Straussberg R, Swoboda KJ, Suri M, Tacke U, Tan TY, te Water Naude J, Wee Teik K, Thomas MM, Till M, Tonduti D, Valente EM, Van Coster RN, van der Knaap MS, Vassallo G, Vijzelaar R, Vogt J, Wallace GB, Wassmer E, Webb HJ, Whitehouse WP, Whitney RN, Zaki MS, Zuberi SM, Livingston JH, Rozenberg F, Lebon P, Vanderver A, Orcesi S, Rice GI (2015) Characterization of human disease phenotypes associated with mutations in TREX1, RNASEH2A, RNASEH2B, RNASEH2C, SAMHD1, ADAR, and IFIH1. *American journal of medical genetics Part A* **167A:** 296-312

Crow YJ, Hayward BE, Parmar R, Robins P, Leitch A, Ali M, Black DN, van Bokhoven H, Brunner HG, Hamel BC, Corry PC, Cowan FM, Frints SG, Klepper J, Livingston JH, Lynch SA, Massey RF, Meritet JF, Michaud JL, Ponsot G, Voit T, Lebon P, Bonthron DT, Jackson AP, Barnes DE, Lindahl T (2006a) Mutations in the gene encoding the 3'-5' DNA exonuclease TREX1 cause Aicardi-Goutieres syndrome at the AGS1 locus. *Nat Genet* **38:** 917-920

Crow YJ, Leitch A, Hayward BE, Garner A, Parmar R, Griffith E, Ali M, Semple C, Aicardi J, Babul-Hirji R, Baumann C, Baxter P, Bertini E, Chandler KE, Chitayat D, Cau D, Dery C, Fazzi E, Goizet C, King MD, Klepper J, Lacombe D, Lanzi G, Lyall H, Martinez-Frias ML, Mathieu M, McKeown C, Monier A, Oade Y, Quarrell OW, Rittey CD, Rogers RC, Sanchis A, Stephenson JB, Tacke U, Till M, Tolmie JL, Tomlin P, Voit T, Weschke B, Woods CG, Lebon P, Bonthron DT, Ponting CP, Jackson AP (2006b) Mutations in genes encoding ribonuclease H2 subunits cause Aicardi-Goutieres syndrome and mimic congenital viral brain infection. *Nat Genet* **38:** 910-916

Crow YJ, Manel N (2015) Aicardi-Goutieres syndrome and the type I interferonopathies. *Nature reviews Immunology* **15:** 429-440

Dmitriev SE, Andreev DE, Terenin IM, Olovnikov IA, Prassolov VS, Merrick WC, Shatsky IN (2007) Efficient translation initiation directed by the 900-nucleotide-long and GC-rich 5' untranslated region of the human retrotransposon LINE-1 mRNA is strictly cap dependent rather than internal ribosome entry site mediated. *Mol Cell Biol* **27:** 4685-4697

Doolittle RF, Feng DF, Johnson MS, McClure MA (1989) Origins and evolutionary relationships of retroviruses. *The Quarterly review of biology* **64:** 1-30

Dornan D, Eckert M, Wallace M, Shimizu H, Ramsay E, Hupp TR, Ball KL (2004) Interferon regulatory factor 1 binding to p300 stimulates DNA-dependent acetylation of p53. *Mol Cell Biol* **24:** 10083-10098

Doucet AJ, Wilusz JE, Miyoshi T, Liu Y, Moran JV (2015) A 3' Poly(A) Tract Is Required for LINE-1 Retrotransposition. *Mol Cell* **60:** 728-741

Esnault C, Casella JF, Heidmann T (2002) A Tetrahymena thermophila ribozyme-based indicator gene to detect transposition of marked retroelements in mammalian cells. *Nucleic Acids Res* **30:** e49

Feng Q, Moran JV, Kazazian HH, Jr., Boeke JD (1996) Human L1 retrotransposon encodes a conserved endonuclease required for retrotransposition. *Cell* **87:** 905-916

Freeman JD, Goodchild NL, Mager DL (1994) A modified indicator gene for selection of retrotransposition events in mammalian cells. *Biotechniques* **17:** 46, 48-49, 52

Garcia Perez JL, Alarcon-Riquelme ME (2017) The TREX1 Dinosaur Bites the Brain through the LINE. *Cell Stem Cell* **21:** 287-288

Garcia-Perez JL, Morell M, Scheys JO, Kulpa DA, Morell S, Carter CC, Hammer GD, Collins KL, O'Shea KS, Menendez P, Moran JV (2010) Epigenetic silencing of engineered L1 retrotransposition events in human embryonic carcinoma cells. *Nature* **466:** 769-773

Garcia-Perez JL, Widmann TJ, Adams IR (2016) The impact of transposable elements on mammalian development. *Development* **143:** 4101-4114

Genovesio A, Kwon YJ, Windisch MP, Kim NY, Choi SY, Kim HC, Jung S, Mammano F, Perrin V, Boese AS, Casartelli N, Schwartz O, Nehrbass U, Emans N (2011) Automated genome-wide visual profiling of cellular proteins involved in HIV infection. *Journal of biomolecular screening* **16:** 945-958

Goodier JL, Zhang L, Vetter MR, Kazazian HH, Jr. (2007) LINE-1 ORF1 protein localizes in stress granules with other RNA-binding proteins, including components of RNA interference RNA-induced silencing complex. *Mol Cell Biol* **27:** 6469-6483

Hancks DC, Kazazian HH, Jr. (2012) Active human retrotransposons: variation and disease. *Current opinion in genetics & development* **22:** 191-203

Heras SR, Macias S, Caceres JF, Garcia-Perez JL (2014) Control of mammalian retrotransposons by cellular RNA processing activities. *Mobile genetic elements* **4:** e28439

Heras SR, Macias S, Plass M, Fernandez N, Cano D, Eyras E, Garcia-Perez JL, Caceres JF (2013) The Microprocessor controls the activity of mammalian retrotransposons. *Nat Struct Mol Biol* **20:** 1173-1181

Hiller B, Achleitner M, Glage S, Naumann R, Behrendt R, Roers A (2012) Mammalian RNase H2 removes ribonucleotides from DNA to maintain genome integrity. *The Journal of experimental medicine* **209:** 1419-1426

Ivics Z, Hackett PB, Plasterk RH, Izsvak Z (1997) Molecular reconstruction of Sleeping Beauty, a bogersposon from fish, and its transposition in human cells. *Cell* **91:** 501-510

Jurka J (1997) Sequence patterns indicate an enzymatic involvement in integration of mammalian retroposons. *Proc Natl Acad Sci U S A* **94:** 1872-1877

Kazazian HH, Jr., Wong C, Youssoufian H, Scott AF, Phillips DG, Antonarakis SE (1988) Haemophilia A resulting from de novo insertion of L1 sequences represents a novel mechanism for mutation in man. *Nature* **332:** 164-166

Kennedy EM, Amie SM, Bambara RA, Kim B (2012) Frequent incorporation of ribonucleotides during HIV-1 reverse transcription and their attenuated repair in macrophages. *J Biol Chem* **287:** 14280-14288

Keskin H, Shen Y, Huang F, Patel M, Yang T, Ashley K, Mazin AV, Storici F (2014) Transcript-RNA-templated DNA recombination and repair. *Nature* **515:** 436-439

Khazina E, Weichenrieder O (2009) Non-LTR retrotransposons encode noncanonical RRM domains in their first open reading frame. *Proc Natl Acad Sci U S A* **106:** 731-736

Kim N, Cho JE, Li YC, Jinks-Robertson S (2013) RNAratioDNA hybrids initiate quasi-palindrome-associated mutations in highly transcribed yeast DNA. *PLoS genetics* **9:** e1003924

Kim N, Huang SN, Williams JS, Li YC, Clark AB, Cho JE, Kunkel TA, Pommier Y, Jinks-Robertson S (2011) Mutagenic processing of ribonucleotides in DNA by yeast topoisomerase I. *Science* **332:** 1561-1564

Kimberland ML, Divoky V, Prchal J, Schwahn U, Berger W, Kazazian HH, Jr. (1999) Full-length human L1 insertions retain the capacity for high frequency retrotransposition in cultured cells. *Hum Mol Genet* **8:** 1557-1560

Kind B, Muster B, Staroske W, Herce HD, Sachse R, Rapp A, Schmidt F, Koss S, Cardoso MC, Lee-Kirsch MA (2014) Altered spatio-temporal dynamics of RNase H2 complex assembly at replication and repair sites in Aicardi-Goutieres syndrome. *Hum Mol Genet* **23:** 5950-5960

Kopera HC, Larson PA, Moldovan JB, Richardson SR, Liu Y, Moran JV (2016) LINE-1 Cultured Cell Retrotransposition Assay. *Methods in molecular biology* **1400:** 139-156

Kopera HC, Moldovan JB, Morrish TA, Garcia-Perez JL, Moran JV (2011) Similarities between LINE-1 reverse transcriptase and telomerase. *Proc Natl Acad Sci U S A* **108:** 20345-20350

Kubo S, Seleme Mdel C, Soifer HS, Perez JL, Moran JV, Kazazian HH, Jr., Kasahara N (2006) L1 retrotransposition in nondividing and primary human somatic cells. *Proc Natl Acad Sci U S A* **103:** 8036-8041

Luan DD, Korman MH, Jakubczak JL, Eickbush TH (1993) Reverse transcription of R2Bm RNA is primed by a nick at the chromosomal target site: a mechanism for non-LTR retrotransposition. *Cell* **72:** 595-605

Macia A, Widmann TJ, Heras SR, Ayllon V, Sanchez L, Benkaddour-Boumzaouad M, Munoz-Lopez M, Rubio A, Amador-Cubero S, Blanco-Jimenez E, Garcia-Castro J, Menendez P, Ng P, Muotri AR, Goodier JL, Garcia-Perez JL (2017) Engineered LINE-1 retrotransposition in nondividing human neurons. *Genome Res* **27:** 335-348

Mackenzie KJ, Carroll P, Lettice L, Tarnauskaite Z, Reddy K, Dix F, Revuelta A, Abbondati E, Rigby RE, Rabe B, Kilanowski F, Grimes G, Fluteau A, Devenney PS, Hill RE, Reijns MA, Jackson AP (2016) Ribonuclease H2 mutations induce a cGAS/STING-dependent innate immune response. *The EMBO journal* **35:** 831-844

Mackenzie KJ, Carroll P, Martin CA, Murina O, Fluteau A, Simpson DJ, Olova N, Sutcliffe H, Rainger JK, Leitch A, Osborn RT, Wheeler AP, Nowotny M, Gilbert N, Chandra T, Reijns MAM, Jackson AP (2017) cGAS surveillance of micronuclei links genome instability to innate immunity. *Nature* **548:** 461-465

Mager DL, Freeman JD (2000) Novel mouse type D endogenous proviruses and ETn elements share long terminal repeat and internal sequences. *J Virol* **74:** 7221-7229

Malik HS, Burke WD, Eickbush TH (1999) The age and evolution of non-LTR retrotransposable elements. *Mol Biol Evol* **16:** 793-805

Martin SL, Bushman FD (2001) Nucleic acid chaperone activity of the ORF1 protein from the mouse LINE-1 retrotransposon. *Mol Cell Biol* **21:** 467-475

Mates L, Chuah MK, Belay E, Jerchow B, Manoj N, Acosta-Sanchez A, Grzela DP, Schmitt A, Becker K, Matrai J, Ma L, Samara-Kuko E, Gysemans C, Pryputniewicz D, Miskey C, Fletcher B, VandenDriessche T, Ivics Z, Izsvak Z (2009) Molecular evolution of a novel hyperactive Sleeping Beauty transposase enables robust stable gene transfer in vertebrates. *Nat Genet* **41:** 753-761

Mathias SL, Scott AF, Kazazian HH, Jr., Boeke JD, Gabriel A (1991) Reverse transcriptase encoded by a human transposable element. *Science* **254:** 1808-1810

Michelini F, Pitchiaya S, Vitelli V, Sharma S, Gioia U, Pessina F, Cabrini M, Wang Y, Capozzo I, Iannelli F, Matti V, Francia S, Shivashankar GV, Walter NG, d'Adda di Fagagna F (2017) Damage-induced lncRNAs control the DNA damage response through interaction with DDRNAs at individual double-strand breaks. *Nature cell biology* **19:** 1400-1411

Moran JV, Holmes SE, Naas TP, DeBerardinis RJ, Boeke JD, Kazazian HH, Jr. (1996) High frequency retrotransposition in cultured mammalian cells. *Cell* **87:** 917-927

Morrish TA, Gilbert N, Myers JS, Vincent BJ, Stamato TD, Taccioli GE, Batzer MA, Moran JV (2002) DNA repair mediated by endonuclease-independent LINE-1 retrotransposition. *Nat Genet* **31:** 159-165

Muotri AR, Chu VT, Marchetto MC, Deng W, Moran JV, Gage FH (2005) Somatic mosaicism in neuronal precursor cells mediated by L1 retrotransposition. *Nature* **435:** 903-910

Nguyen HD, Yadav T, Giri S, Saez B, Graubert TA, Zou L (2017) Functions of Replication Protein A as a Sensor of R Loops and a Regulator of RNaseH1. *Mol Cell* **65:** 832-847 e834

Nick McElhinny SA, Kumar D, Clark AB, Watt DL, Watts BE, Lundstrom EB, Johansson E, Chabes A, Kunkel TA (2010) Genome instability due to ribonucleotide incorporation into DNA. *Nature chemical biology* **6:** 774-781

Ohle C, Tesorero R, Schermann G, Dobrev N, Sinning I, Fischer T (2016) Transient RNA-DNA Hybrids Are Required for Efficient Double-Strand Break Repair. *Cell* **167:** 1001-1013 e1007

Olivares M, Garcia-Perez JL, Thomas MC, Heras SR, Lopez MC (2002) The non-LTR (long terminal repeat) retrotransposon L1Tc from Trypanosoma cruzi codes for a protein with RNase H activity. *J Biol Chem* **277:** 28025-28030

Orecchini E, Doria M, Antonioni A, Galardi S, Ciafre SA, Frassinelli L, Mancone C, Montaldo C, Tripodi M, Michienzi A (2017) ADAR1 restricts LINE-1 retrotransposition. *Nucleic Acids Res* **45:** 155-168

Parajuli S, Teasley DC, Murali B, Jackson J, Vindigni A, Stewart SA (2017) Human ribonuclease H1 resolves R-loops and thereby enables progression of the DNA replication fork. *J Biol Chem* **292:** 15216-15224

Piskareva O, Denmukhametova S, Schmatchenko V (2003) Functional reverse transcriptase encoded by the human LINE-1 from baculovirus-infected insect cells. *Protein Expr Purif* **28:** 125-130

Piskareva O, Schmatchenko V (2006) DNA polymerization by the reverse transcriptase of the human L1 retrotransposon on its own template in vitro. *FEBS Lett* **580:** 661-668

Pizarro JG, Cristofari G (2016) Post-Transcriptional Control of LINE-1 Retrotransposition by Cellular Host Factors in Somatic Cells. *Frontiers in cell and developmental biology* **4:** 14

Potenski CJ, Niu H, Sung P, Klein HL (2014) Avoidance of ribonucleotide-induced mutations by RNase H2 and Srs2-Exo1 mechanisms. *Nature* **511:** 251-254

Ran FA, Hsu PD, Wright J, Agarwala V, Scott DA, Zhang F (2013) Genome engineering using the CRISPR-Cas9 system. *Nat Protoc* **8:** 2281-2308

Reijns MA, Bubeck D, Gibson LC, Graham SC, Baillie GS, Jones EY, Jackson AP (2011) The structure of the human RNase H2 complex defines key interaction interfaces relevant to enzyme function and human disease. *J Biol Chem* **286:** 10530-10539

Reijns MA, Jackson AP (2014) Ribonuclease H2 in health and disease. *Biochem Soc Trans* **42:** 717-725

Reijns MA, Rabe B, Rigby RE, Mill P, Astell KR, Lettice LA, Boyle S, Leitch A, Keighren M, Kilanowski F, Devenney PS, Sexton D, Grimes G, Holt IJ, Hill RE, Taylor MS, Lawson KA, Dorin JR, Jackson AP (2012) Enzymatic removal of ribonucleotides from DNA is essential for mammalian genome integrity and development. *Cell* **149:** 1008-1022

Ribet D, Dewannieux M, Heidmann T (2004) An active murine transposon family pair: retrotransposition of "master" MusD copies and ETn trans-mobilization. *Genome Res* **14:** 2261-2267

Rice GI, Bond J, Asipu A, Brunette RL, Manfield IW, Carr IM, Fuller JC, Jackson RM, Lamb T, Briggs TA, Ali M, Gornall H, Couthard LR, Aeby A, Attard-Montalto SP, Bertini E, Bodemer C, Brockmann K, Brueton LA, Corry PC, Desguerre I, Fazzi E, Cazorla AG, Gener B, Hamel BC, Heiberg A, Hunter M, van der Knaap MS, Kumar R, Lagae L, Landrieu PG, Lourenco CM, Marom D, McDermott MF, van der Merwe W, Orcesi S, Prendiville JS, Rasmussen M, Shalev SA, Soler DM, Shinawi M, Spiegel R, Tan TY, Vanderver A, Wakeling EL, Wassmer E, Whittaker E, Lebon P, Stetson DB, Bonthron DT, Crow YJ (2009) Mutations involved in Aicardi-Goutieres syndrome implicate SAMHD1 as regulator of the innate immune response. *Nat Genet* **41:** 829-832

Rice GI, Del Toro Duany Y, Jenkinson EM, Forte GM, Anderson BH, Ariaudo G, Bader-Meunier B, Baildam EM, Battini R, Beresford MW, Casarano M, Chouchane M, Cimaz R, Collins AE, Cordeiro NJ, Dale RC, Davidson JE, De Waele L, Desguerre I, Faivre L, Fazzi E, Isidor B, Lagae L, Latchman AR, Lebon P, Li C, Livingston JH, Lourenco CM, Mancardi MM, Masurel-Paulet A, McInnes IB, Menezes MP, Mignot C, O'Sullivan J, Orcesi S, Picco PP, Riva E, Robinson RA, Rodriguez D, Salvatici E, Scott C, Szybowska M, Tolmie JL, Vanderver A, Vanhulle C, Vieira JP, Webb K, Whitney RN, Williams SG, Wolfe LA, Zuberi SM, Hur S, Crow YJ (2014) Gain-of-function mutations in IFIH1 cause a spectrum of human disease phenotypes associated with upregulated type I interferon signaling. *Nat Genet* **46:** 503-509

Rice GI, Forte GM, Szynkiewicz M, Chase DS, Aeby A, Abdel-Hamid MS, Ackroyd S, Allcock R, Bailey KM, Balottin U, Barnerias C, Bernard G, Bodemer C, Botella MP, Cereda C, Chandler KE, Dabydeen L, Dale RC, De Laet C, De Goede CG, Del Toro M, Effat L, Enamorado NN, Fazzi E, Gener B, Haldre M, Lin JP, Livingston JH, Lourenco CM, Marques W, Jr., Oades P, Peterson P, Rasmussen M, Roubertie A, Schmidt JL, Shalev SA, Simon R, Spiegel R, Swoboda KJ, Temtamy SA, Vassallo G, Vilain CN, Vogt J, Wermenbol V, Whitehouse WP, Soler D, Olivieri I, Orcesi S, Aglan MS, Zaki MS, Abdel-Salam GM, Vanderver A, Kisand K, Rozenberg F, Lebon P, Crow YJ (2013) Assessment of interferon-related biomarkers in Aicardi-Goutieres syndrome associated with mutations in TREX1, RNASEH2A, RNASEH2B, RNASEH2C, SAMHD1, and ADAR: a case-control study. *The Lancet Neurology* **12:** 1159-1169

Rice GI, Kasher PR, Forte GM, Mannion NM, Greenwood SM, Szynkiewicz M, Dickerson JE, Bhaskar SS, Zampini M, Briggs TA, Jenkinson EM, Bacino CA, Battini R, Bertini E, Brogan PA, Brueton LA, Carpanelli M, De Laet C, de Lonlay P, del Toro M, Desguerre I, Fazzi E, Garcia-Cazorla A, Heiberg A, Kawaguchi M, Kumar R, Lin JP, Lourenco CM, Male AM, Marques W, Jr., Mignot C, Olivieri I, Orcesi S, Prabhakar P, Rasmussen M, Robinson RA, Rozenberg F, Schmidt JL, Steindl K, Tan TY, van der Merwe WG, Vanderver A, Vassallo G, Wakeling EL, Wassmer E, Whittaker E, Livingston JH, Lebon P, Suzuki T, McLaughlin PJ, Keegan LP, O'Connell MA, Lovell SC, Crow YJ (2012) Mutations in ADAR1 cause Aicardi-Goutieres syndrome associated with a type I interferon signature. *Nat Genet* **44:** 1243-1248

Richardson SR, Doucet AJ, Kopera HC, Moldovan JB, Garcia-Perez JL, Moran JV (2015) The Influence of LINE-1 and SINE Retrotransposons on Mammalian Genomes. *Microbiology spectrum* **3:** MDNA3-0061-2014

Richardson SR, Narvaiza I, Planegger RA, Weitzman MD, Moran JV (2014) APOBEC3A deaminates transiently exposed single-strand DNA during LINE-1 retrotransposition. *eLife* **3**

Sassaman DM, Dombroski BA, Moran JV, Kimberland ML, Naas TP, DeBerardinis RJ, Gabriel A, Swergold GD, Kazazian HH, Jr. (1997) Many human L1 elements are capable of retrotransposition. *Nat Genet* **16:** 37-43

Scott AF, Schmeckpeper BJ, Abdelrazik M, Comey CT, O'Hara B, Rossiter JP, Cooley T, Heath P, Smith KD, Margolet L (1987) Origin of the human L1 elements: proposed progenitor genes deduced from a consensus DNA sequence. *Genomics* **1:** 113-125

Shen W, Sun H, De Hoyos CL, Bailey JK, Liang XH, Crooke ST (2017) Dynamic nucleoplasmic and nucleolar localization of mammalian RNase H1 in response to RNAP I transcriptional R-loops. *Nucleic Acids Res* **45:** 10672-10692

Sparks JL, Chon H, Cerritelli SM, Kunkel TA, Johansson E, Crouch RJ, Burgers PM (2012) RNase H2-initiated ribonucleotide excision repair. *Mol Cell* **47:** 980-986

Stetson DB, Ko JS, Heidmann T, Medzhitov R (2008) Trex1 prevents cell-intrinsic initiation of autoimmunity. *Cell* **134:** 587-598

Sugano T, Kajikawa M, Okada N (2006) Isolation and characterization of retrotransposition-competent LINEs from zebrafish. *Gene* **365:** 74-82

Swergold GD (1990) Identification, characterization, and cell specificity of a human LINE-1 promoter. *Mol Cell Biol* **10:** 6718-6729

Swift S, Lorens J, Achacoso P, Nolan GP (2001) Rapid production of retroviruses for efficient gene delivery to mammalian cells using 293T cell-based systems. *Current protocols in immunology* **Chapter 10:** Unit 10 17C

Taylor MS, Lacava J, Mita P, Molloy KR, Huang CR, Li D, Adney EM, Jiang H, Burns KH, Chait BT, Rout MP, Boeke JD, Dai L (2013) Affinity Proteomics Reveals Human Host Factors Implicated in Discrete Stages of LINE-1 Retrotransposition. *Cell* **155:** 1034-1048

Thomas CA, Tejwani L, Trujillo CA, Negraes PD, Herai RH, Mesci P, Macia A, Crow YJ, Muotri AR (2017) Modeling of TREX1-Dependent Autoimmune Disease using Human Stem Cells Highlights L1 Accumulation as a Source of Neuroinflammation. *Cell Stem Cell* **21:** 319-331 e318

Upton KR, Gerhardt DJ, Jesuadian JS, Richardson SR, Sanchez-Luque FJ, Bodea GO, Ewing AD, Salvador-Palomeque C, van der Knaap MS, Brennan PM, Vanderver A, Faulkner GJ (2015) Ubiquitous L1 mosaicism in hippocampal neurons. *Cell* **161:** 228-239

Volkman HE, Stetson DB (2014) The enemy within: endogenous retroelements and autoimmune disease. *Nature immunology* **15:** 415-422

Wei W, Gilbert N, Ooi SL, Lawler JF, Ostertag EM, Kazazian HH, Boeke JD, Moran JV (2001) Human L1 retrotransposition: cis preference versus trans complementation. *Mol Cell Biol* **21:** 1429-1439

Wei W, Morrish TA, Alisch RS, Moran JV (2000) A transient assay reveals that cultured human cells can accommodate multiple LINE-1 retrotransposition events. *Anal Biochem* **284:** 435-438

Xie Y, Rosser JM, Thompson TL, Boeke JD, An W (2011) Characterization of L1 retrotransposition with high-throughput dual-luciferase assays. *Nucleic Acids Res* **39:** e16

Zhao K, Du J, Han X, Goodier JL, Li P, Zhou X, Wei W, Evans SL, Li L, Zhang W, Cheung LE, Wang G, Kazazian HH, Jr., Yu XF (2013) Modulation of LINE-1 and Alu/SVA retrotransposition by Aicardi-Goutieres syndrome-related SAMHD1. *Cell reports* **4:** 1108-1115

Figure 1

A

RNASEH2A
RNASEH2B
RNASEH2C
Tubulin

parental C1 C2 KO1 KO2 KO3 parental | parental C3 C4 C6 KO4 KO5 KO6 C5 parental

B

DRD:DNA

Activity (% of parental)

Controls   KO

C

parental C1 C2 KO1 KO2 KO3 parental | parental C3 C4 C6 KO4 KO5 KO6 parental

kb
10
8
6
5
4
3

2

1

D

Human LINE-1 (JJ101/L1.3)

CMV 5' UTR ORF1 ORF2
EN RT C
AST BL

E

% Retrotransposition (TE normalised)

**

Controls   KO

F

WT-hL1 (L1.3) ENm-hL1 (D205A) RTm-hL1 (D702A)   WT-hL1 (L1.3) ENm-hL1 (D205A) RTm-hL1 (D702A)

Parental
C1   KO1
C2   KO2
C3   KO3
C4   KO4
C5   KO5
C6   KO6

Figure 2

A — U2OS

RNASEH2A
RNASEH2B
RNASEH2C
Vinculin

Parental, KO1, KO2, C1

B

DRD:DNA

Activity (% of parental)

Parental, KO1, KO2, C1

C

kb
10
8
6
5
4
3

2

1

Parental, C1, KO1, KO2

D

Human LINE-1 (JJ101/L1.3)

CMV 5' UTR ORF1 ORF2 EN RT C AST BL

WT-hL1 (L1.3)   RTm-hL1 (D702A)   CTRL (pcDNA6.1)

Parental

C1

KO1

KO2

% Retrotransposition (TE normalized)

94 ± 8.2

Average:
25 ± 9.5

parental, C1, KO1, KO2

Figure 3

A

Human LINE-1 (JJ101/L1.3)

HeLa

WT-hL1 (L1.3) ENm-hL1 (D205A) RTm-hL1 (D702A) CTRL (pcDNA6.1)

-ve (β-arrestin)

RNase H2 (1:1:1)

+ve (APOBEC3A)

***

% Retrotransposition

-ve   RNase H2   +ve

B

Human LINE-1 (JJ101/L1.3)

U2OS

WT-hL1 (L1.3) ENm-hL1 (D205A) RTm-hL1 (D702A) CTRL (pcDNA6.1)

-ve (β-arrestin)

RNase H2 (1:1:1)

+ve (APOBEC3A)

**

% Retrotransposition

-ve   RNase H2   +ve

Figure 4

Figure 5

Figure 6

Figure 7

Figure EV1

A

Zebrafish LINE-2 (Zfl2-2mneol**)**

Human LINE-1 (JM101/L1.3)

B

U2OS

Average:
hL1: **111** ± 7.8
zL2: **105** ± 3.5

Average:
hL1: **8.0** ± 0.07
zL2: **14** ± 2.4

A

HeLa   **U2OS**   Figure EV3

Anti-V5

b-actin (42 KDa) ▶

B

Human LINE-1 (JJ101/L1.3)

HeLa

C

Human LINE-1 (JJ101/L1.3)

U2OS
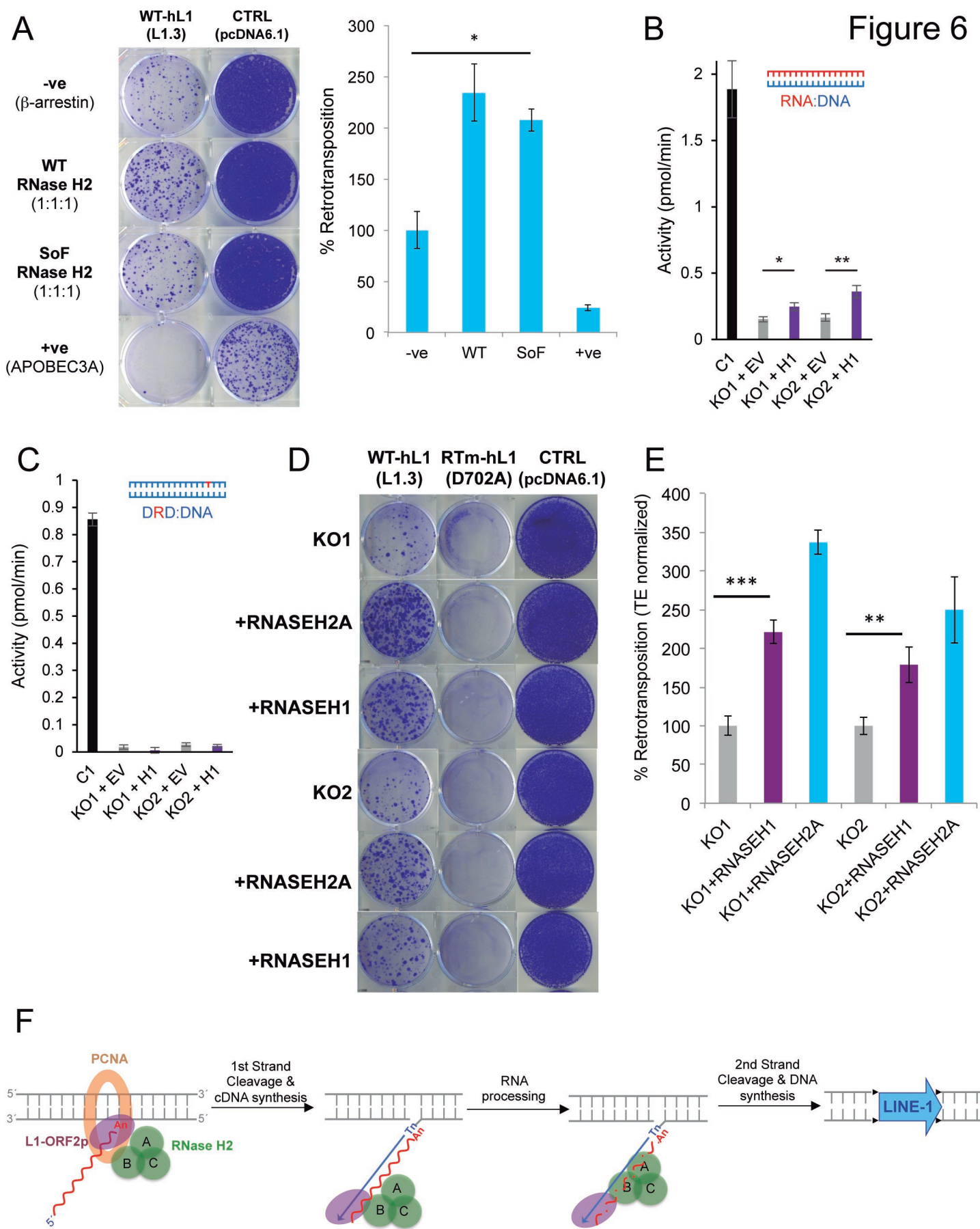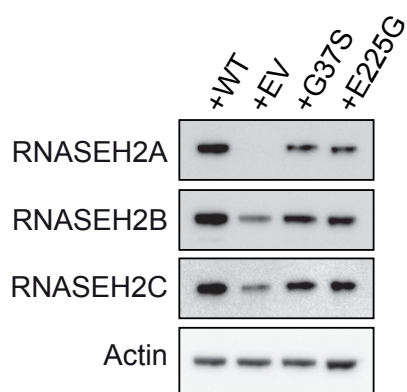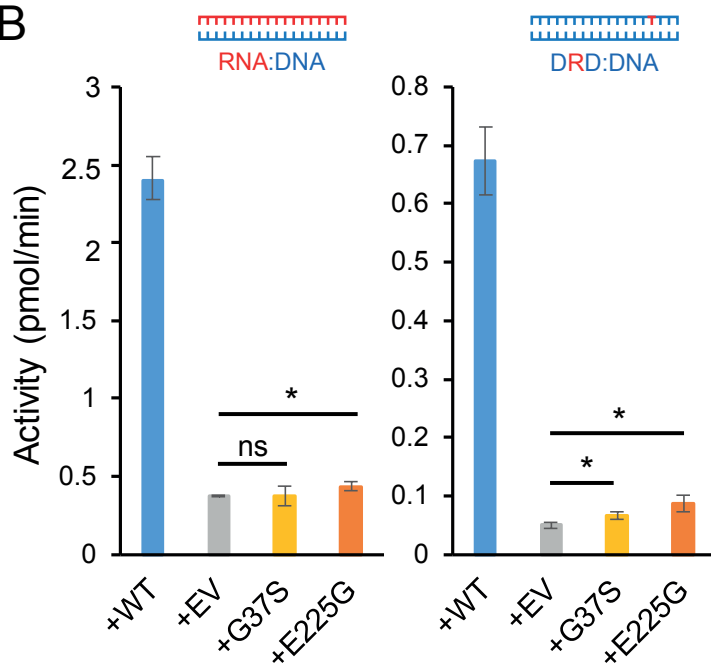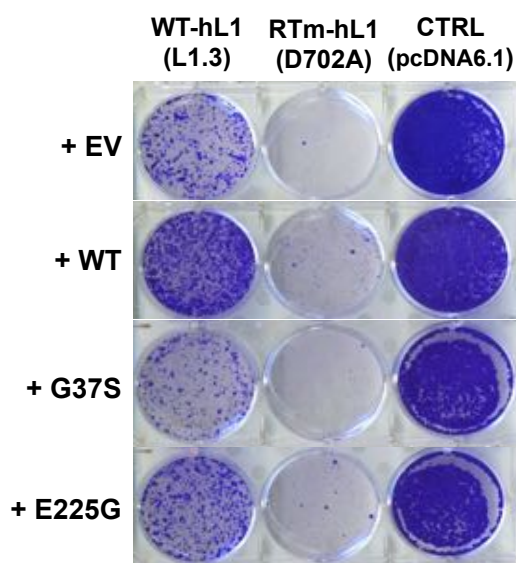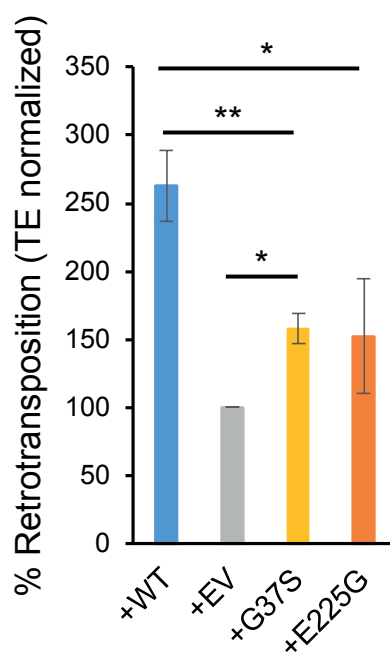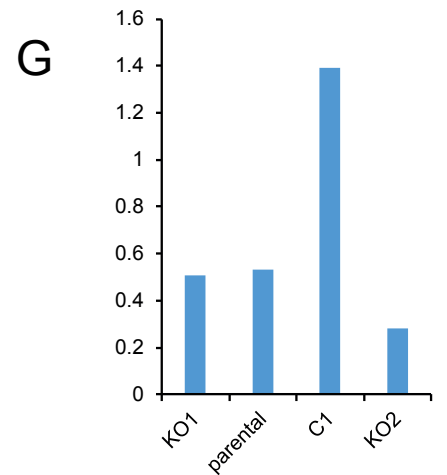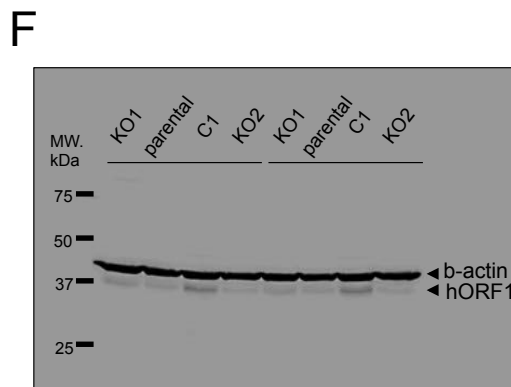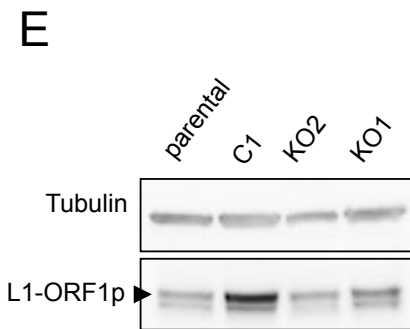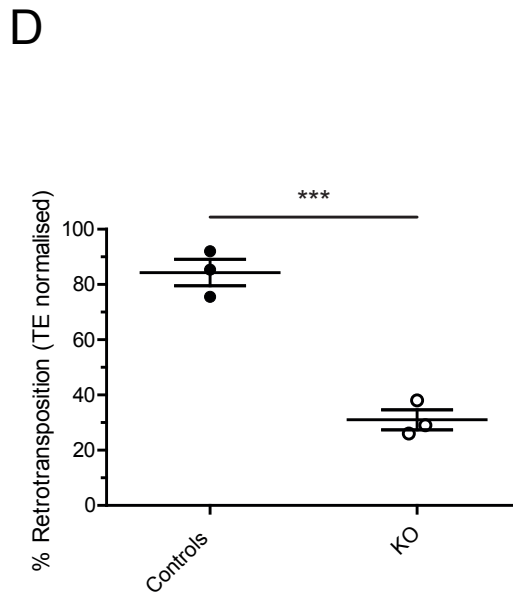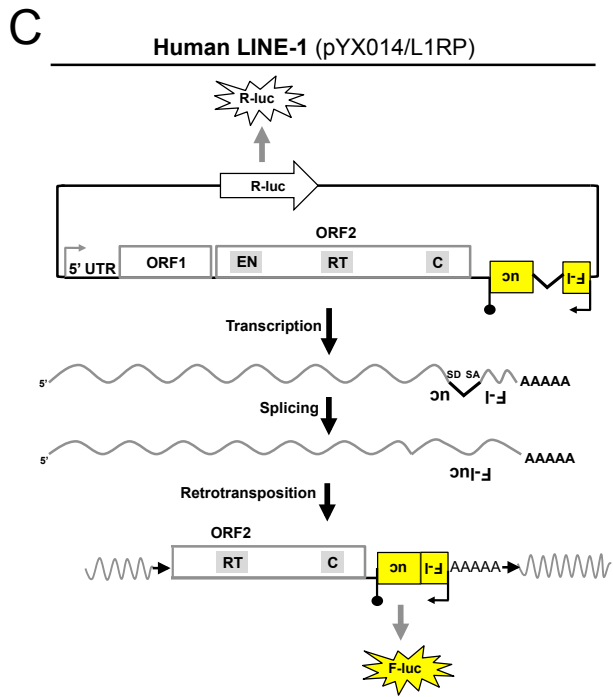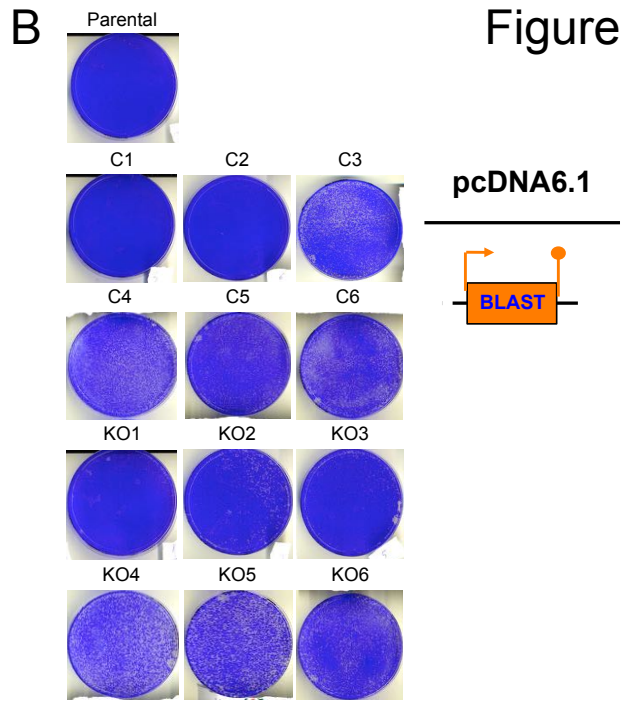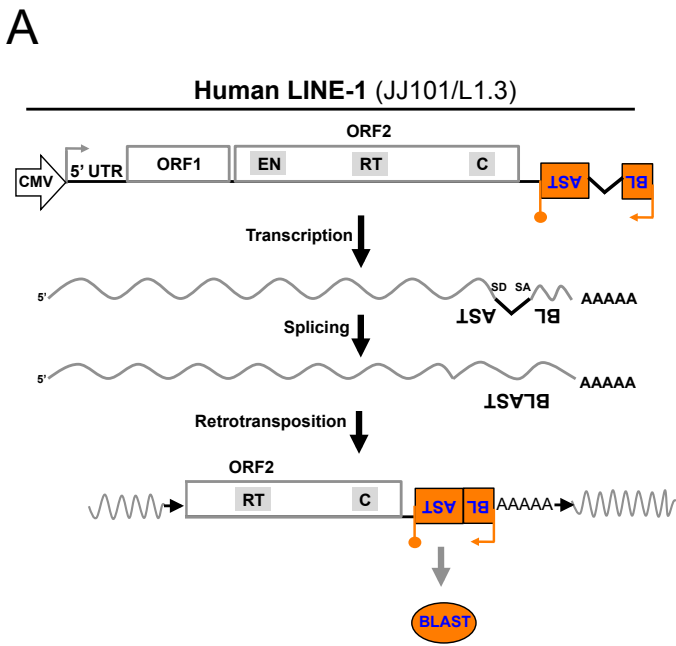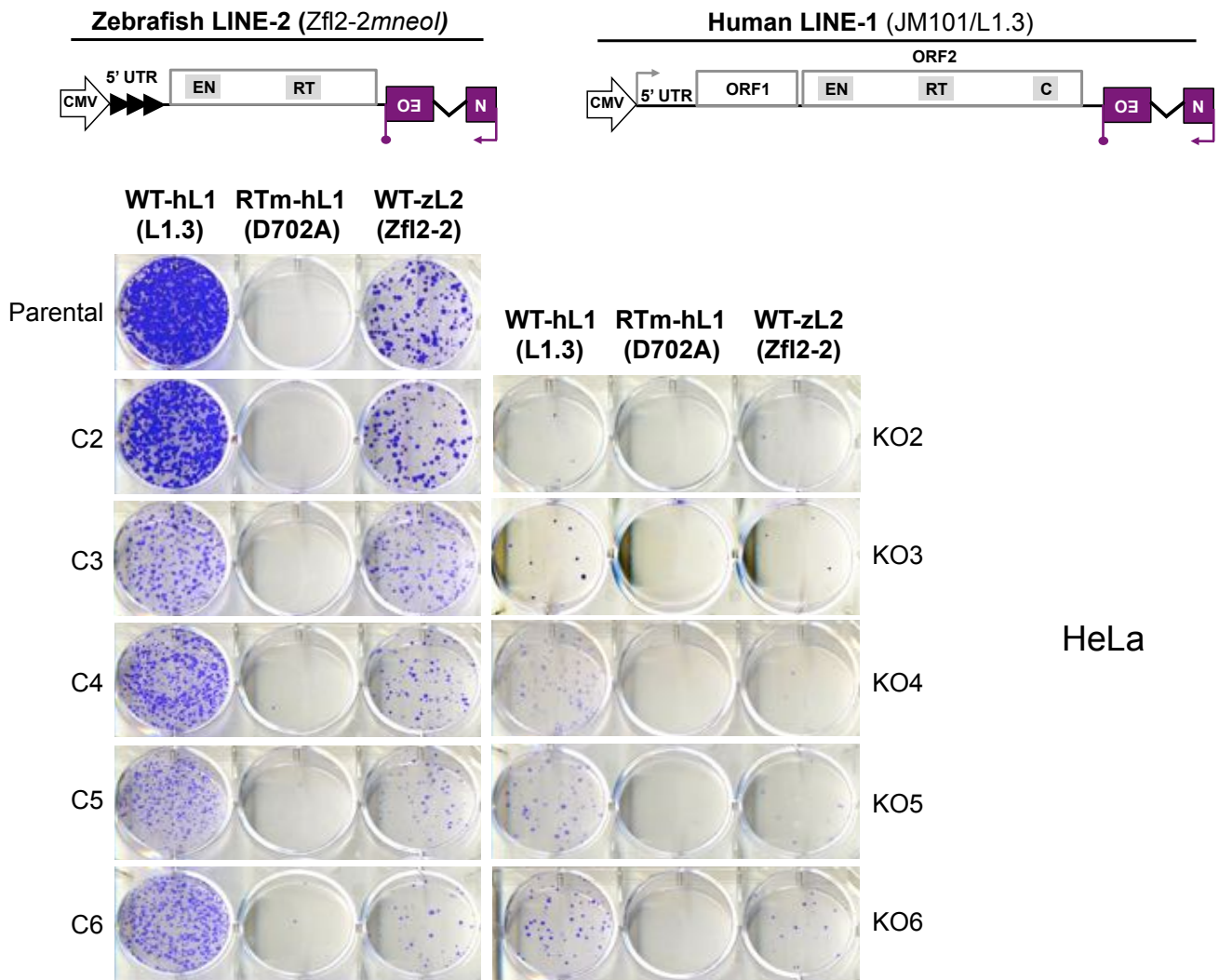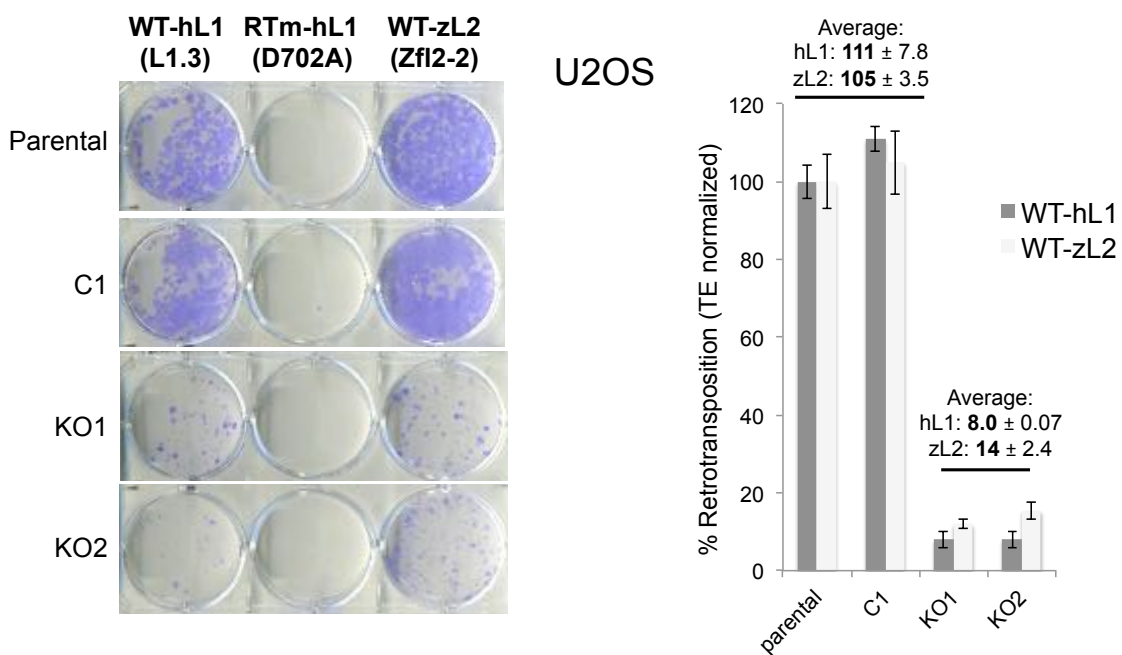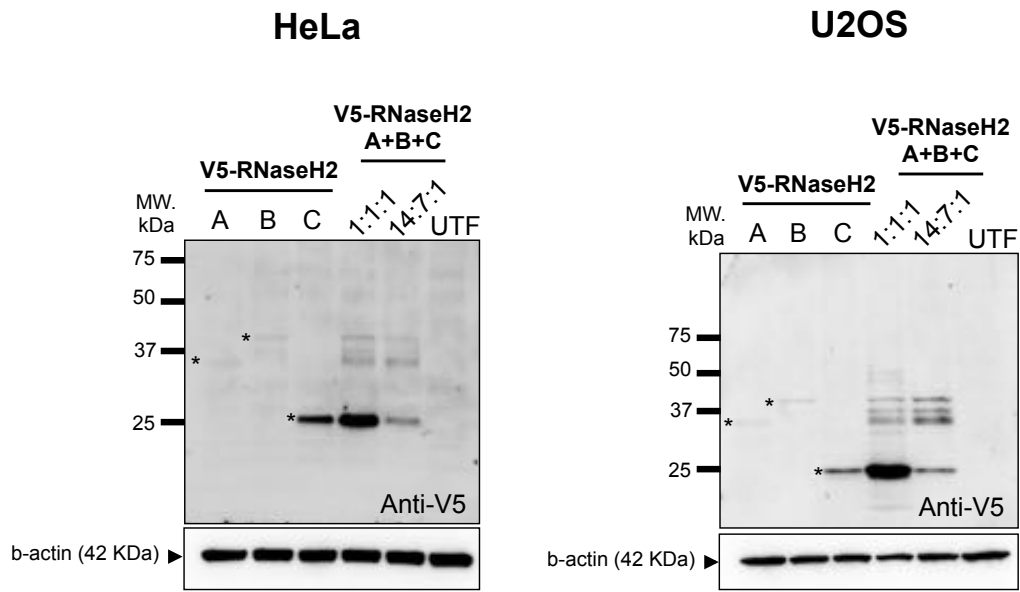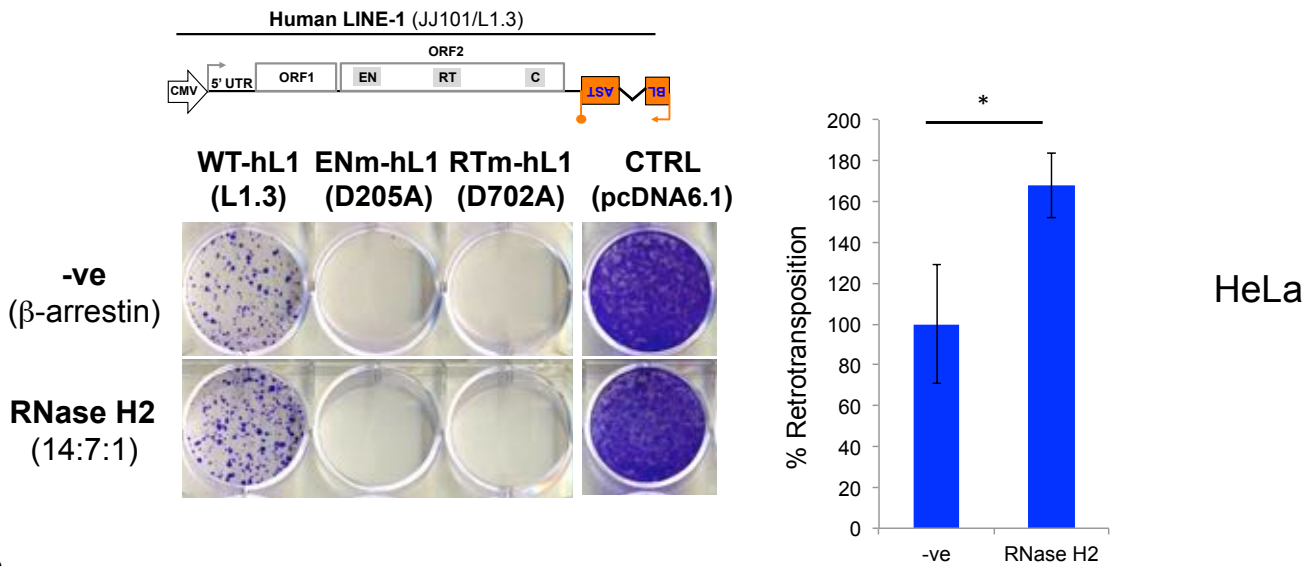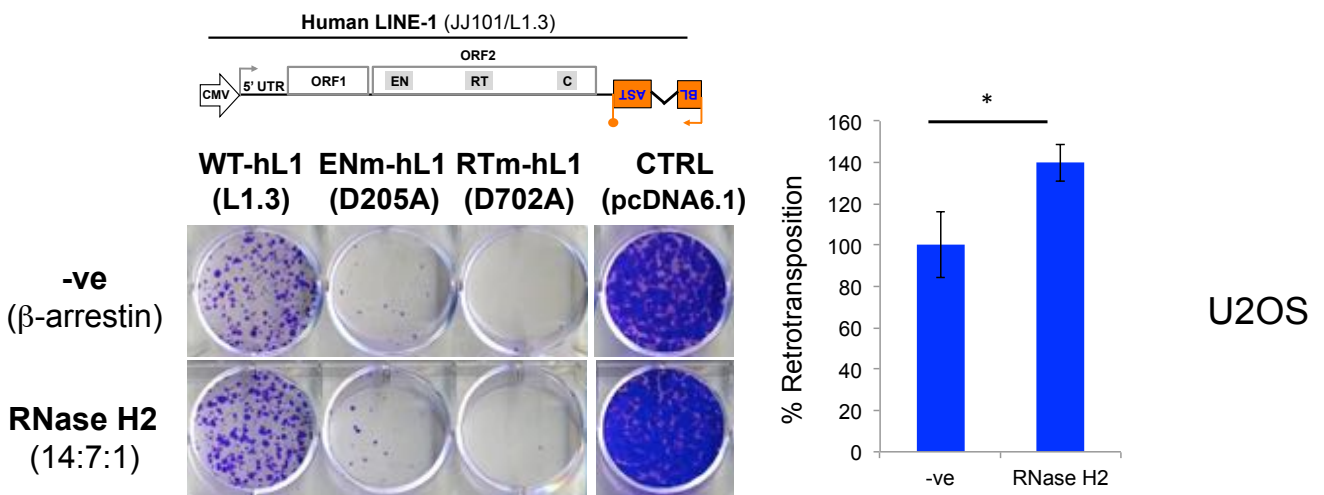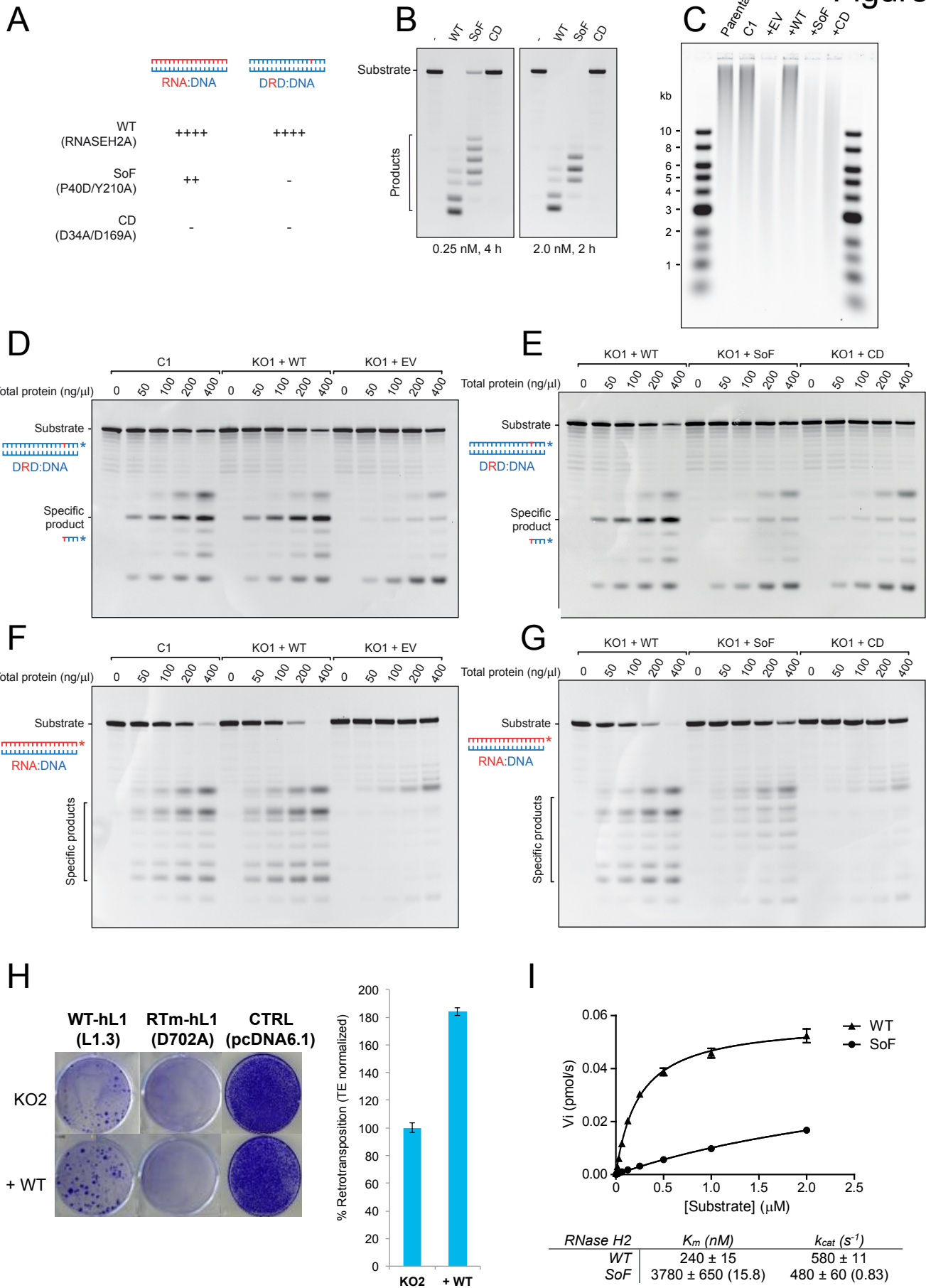
A
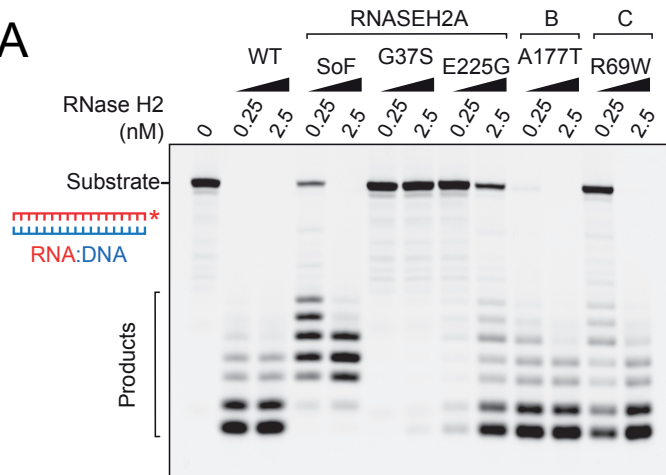
B
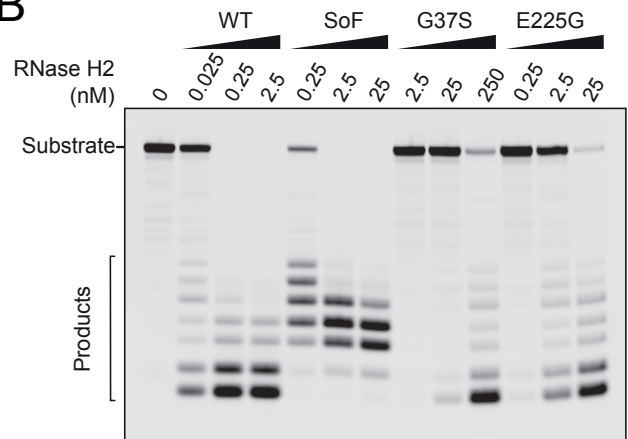
APPENDIX

RNase H2, mutated in Aicardi-Goutières syndrome, promotes LINE-1 retrotransposition

Maria Benitez-Guijarro, Cesar Lopez-Ruiz, Žygimantė Tarnauskaitė, Olga Murina, Mahwish Mian Mohammad, Thomas C. Williams, Adeline Fluteau, Laura Sanchez, Raquel Vilar-Astasio, Marta Garcia-Canadas, David Cano, Marie-Jeanne H. C. Kempen, Antonio Sanchez-Pozo, Sara R. Heras, Andrew P. Jackson, Martin A. M. Reijns[*] and Jose L. Garcia-Perez[*]

Contents:

Appendix Figure S1. Reduced LINE-1 retrotransposition in RNase H2 null HCT116 p53$^{-/-}$ cells

A. Western blot analysis shows absence of RNASEH2A and reduced RNASEH2B and C in RNASEH2A-KO clones (KO1, KO2), compared to control clones (C1-4). Tubulin was used as a loading control. See also Source data.

B. RNase H assay shows absence of activity against single embedded ribonucleotides in KO clones, compared to control cells. Mean ± SD for n= 3 independent experiments.

C. High levels of genome embedded ribonucleotides in HCT116 p53$^{-/-}$ RNASEH2-KO clones. Genomic DNA was isolated from control and KO clones, RNase H2 treated and separated by alkaline gel electrophoresis. Smaller fragments indicate more genome embedded ribonucleotides.

D. Schematic of plasmid JJ101/L1.3, and representative retrotransposition and toxicity assays conducted in HCT116 p53$^{-/-}$ control clones (C1-4), and in two RNASEH2A-KO clones (KO1 and KO2). Cells were transfected with active human LINE-1 (WT-hL1, element L1.3), RT-mutant LINE-1 (RTm-hL1, D702A), or a toxicity control vector (CTRL, pcDNA6.1).

E. Quantification of L1-WT retrotransposition, with average retrotransposition in control cells set to 100% for comparison, shows reduced activity in RNase H2 null cells. Dots represent the mean of 3 technical replicates for individual clones. Lines indicate the mean of n=4 biological replicates for controls (C1-4) and n=2 for KO clones (KO1, 2) ± SEM (representative of 5 independent experiments). t-test, **, p<0.01

Appendix Figure S2. RNase H2 activity is dispensable for LTR-retroelement and DNA-Transposon activity

A. Schematic of a neo^{TNF} tagged MusD mouse LTR-retrotransposon. The relative position of the *gag, pro* and *pol* genes is indicated. The purple box with a backward NEO label depicts the retrotransposition indicator cassette neo^{TNF}, and the purple arrow and lollipop indicate the presence of a promoter and polyadenylation signal respectively. Upon transcription from the CMV promoter located upstream of the MusD element, this mRNA can be spliced by canonical *cis*-splicing and undergo a round of LTR-retrotransposition, resulting in the activation of the neo^{TNF} reporter and subsequent translation of the neomycin phosphotransferase protein (purple oval with white NEO label). In the LTR-retrotransposition event shown in the bottom, the black arrows indicate the presence of TSDs flanking the MusD insertion.

B. Representative results of LTR-retrotransposition assays in HeLa control (C1-6) and RNASEH2A KO (KO1-6) clones. Labels indicate if cells were transfected with a tagged active mouse MusD element (MusD) or with the toxicity control plasmid (pU6ineo).

C. Quantification of LTR-retrotransposition assays in U2OS control (C1) and RNASEH2A-KO1 clones. Mean ± SD for n=3 technical replicates (representative of 3 independent experiments).

D. Schematic of the two plasmids used in the Sleeping Beauty transposition assay. The purple box with a NEO label depicts the neo expression cassette. Underneath, quantification of SB assays in U2OS cells. Mean ± SD for n=2 technical replicates (representative of 3 independent experiments).

**Appendix Figure S3. No increased mutation rate in *de novo* LINE-1 insertions in RNase H2 null cells**

A. Schematic of retrotransposition assay using plasmid JM101/L1.3. Red arrows indicate primers, flanking the engineered intron present in *mneoI,* used in the PCR assay. Note the SwaI site in the engineered *mneoI* intron (dashed vertical line), which, when cut, prevents amplification of intron-containing PCR product.

B. Time line of the mutation detection assay.

C. PCR products separated by agarose gel electrophoresis. Products amplified using DNA isolated from WT, KO1 and KO2 cell lines after 2 or 5 days, as indicated; genomic DNA digested with SwaI prior to PCR (see A). C(-), negative control without template DNA. M, marker (1-Kb ladder, molecular weight standard). Arrow indicates the expected PCR product; * indicates product resulting from the use of cryptic splice sites in the Neo coding sequence.

D. Schematic of the spliced *mneoI* cassette, where the presence of tandem repeats are indicated using yellow boxes. The green box (labelled Alternative Intron) indicates the relative position of the cryptic intron. Red arrows indicate the relative position of primers used for PCR.

E. Mutation rate is not increased in RNase H2 deficient cells (-) when compared to RNase H2 proficient control cells (+).

Appendix Figure S4. Increased RNase H activity against RNA:DNA heteroduplexes in RNASEH2A-KO HeLa cells complemented with human RNase H1

A, B. RNase H activity assays conducted on RNASEH2A-KO cells (**A**, KO1; **B**, KO2) complemented with human nuclear RNASEH1 (+RNASEH1) or with empty vector (+EV). RNase H activity was measured using the 18-bp RNA:DNA substrate, separating products by denaturing PAGE after incubation with lysates from the indicated cell lines using increasing amounts of total protein. Left panels, representative gels. Right panels, quantifications showing mean ± SEM of n=4 (KO1) or n=3 (KO2) independent experiments. Mean for n=3 independent experiments. Two-way ANOVA with post-hoc Bonferroni multiple comparison test shows significant increase in activity against RNA:DNA heteroduplexes in KO+RNASEH1 compared to KO+EV cells. ***, $p < 0.001$; ****, $p < 0.0001$

A

HCT116 p53$^{-/-}$

B

Activity (% of WT average)

DRD:DNA

C

kb

D

Human LINE-1 (JJ101/L1.3)

CMV | 5' UTR | ORF1 | ORF2 | EN | RT | C | AST | BL

WT-hL1 (L1.3) | ENm-hL1 (D205A) | CTRL (pcDNA6.1) | WT-hL1 (L1.3) | ENm-hL1 (D205A) | CTRL (pcDNA6.1)

C1 | C4
C2 | KO1
C3 | KO2

E

% Retrotransposition (TE normalised)

**

Controls | KO

A

Mouse LTR-Retrotransposon (MusD-6neoTNF)

B

HeLa
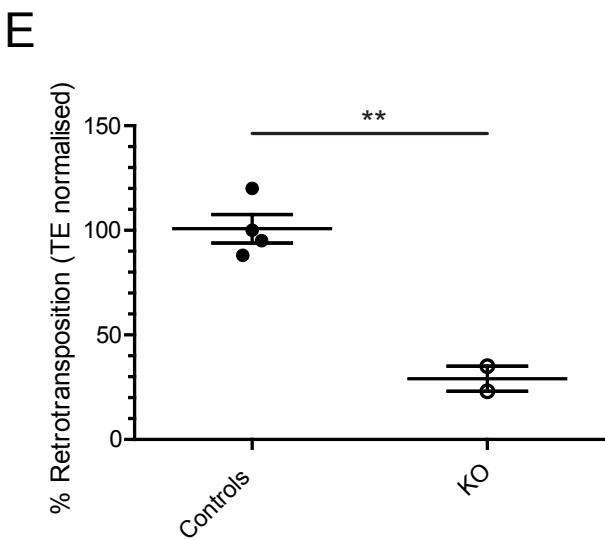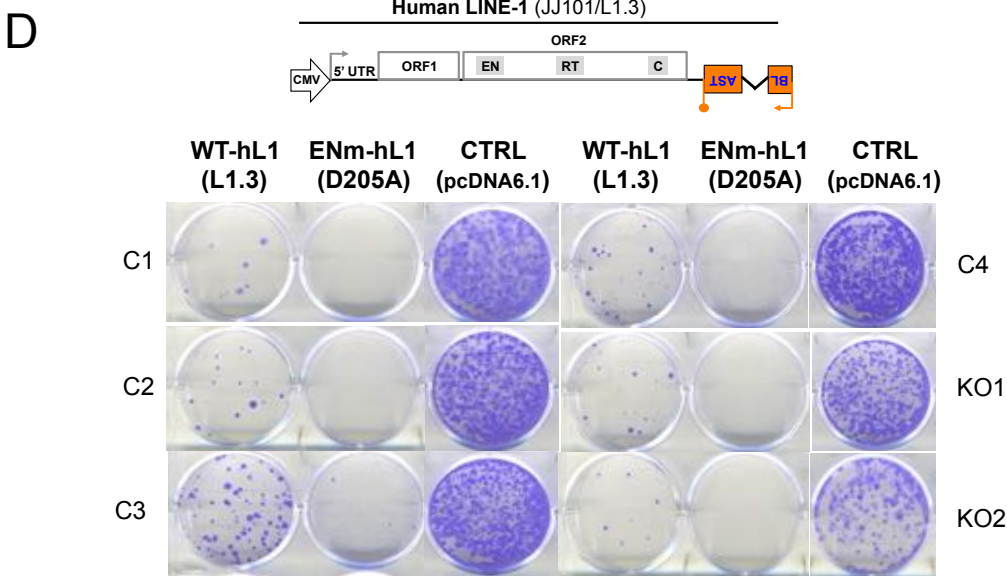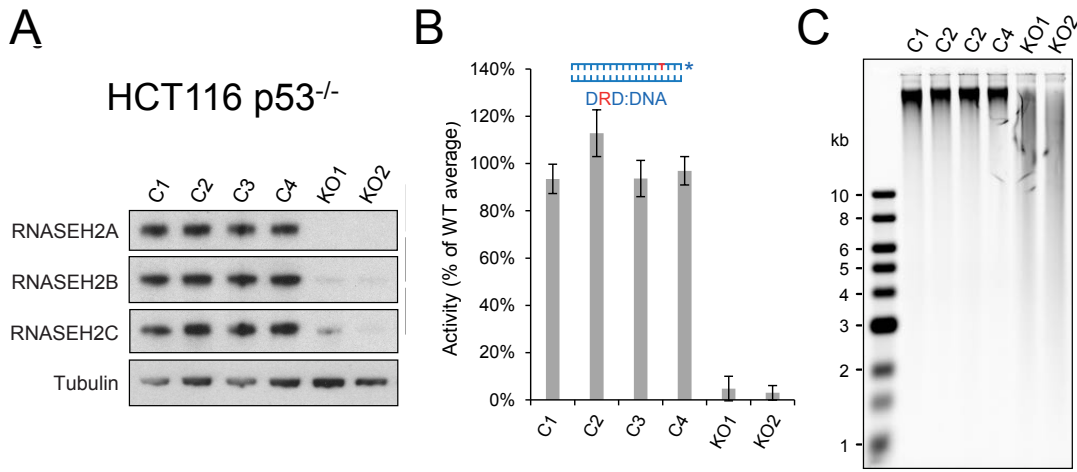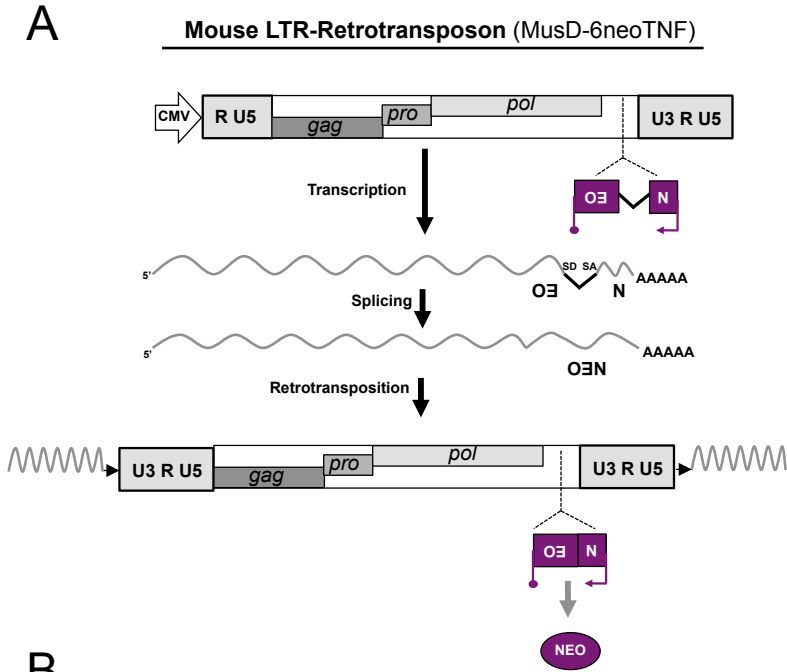
C

Mouse LTR-Retrotransposon (MusD-6neoTNF)

U2OS
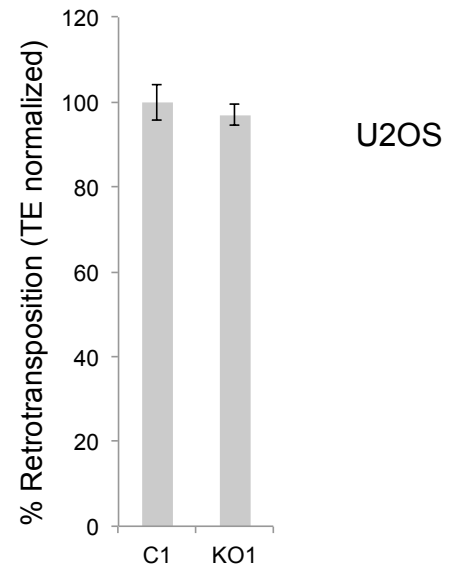
D

Tc-1 DNA-Transposon (Sleeping Beauty)

U2OS

A

Human LINE-1 (JM101/L1.3)

B

C

D
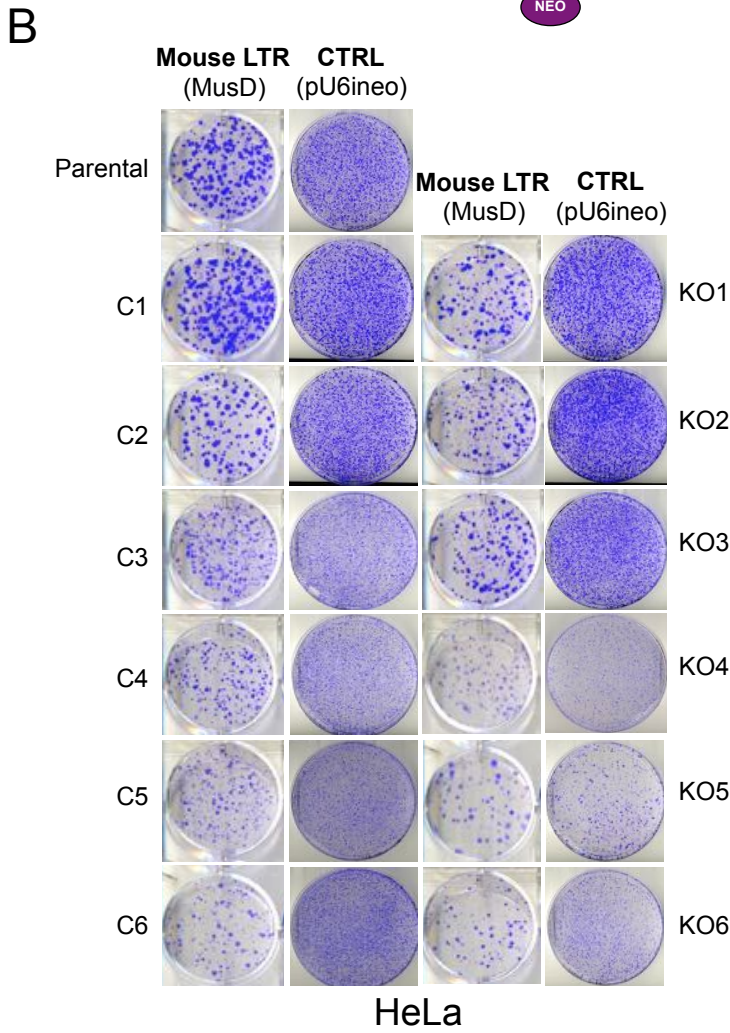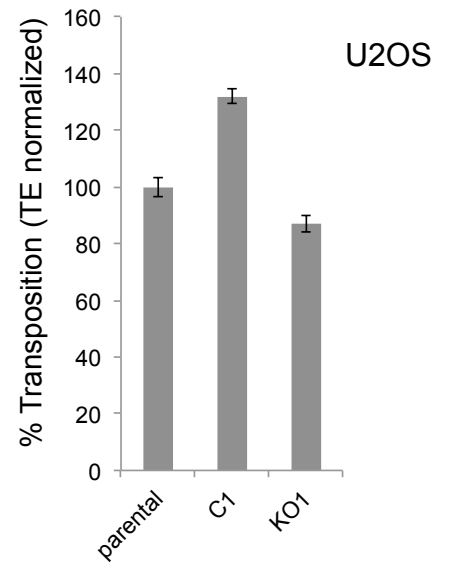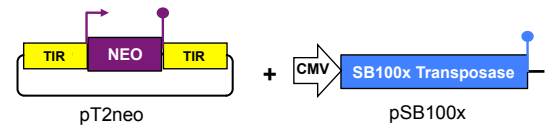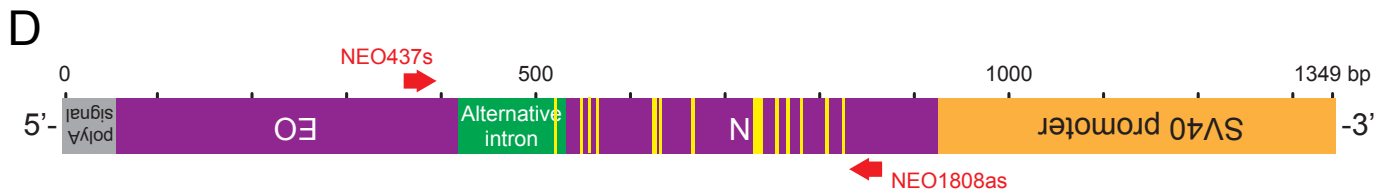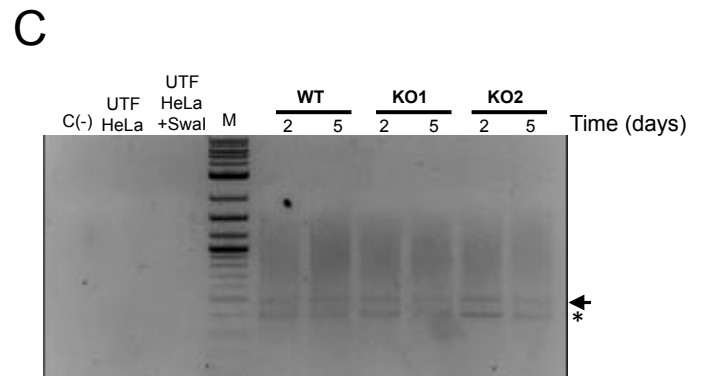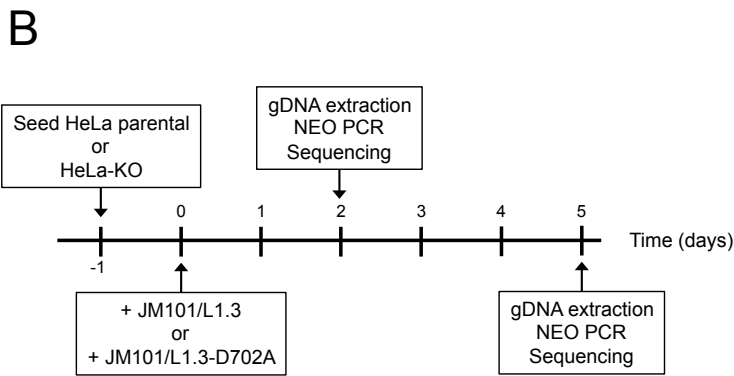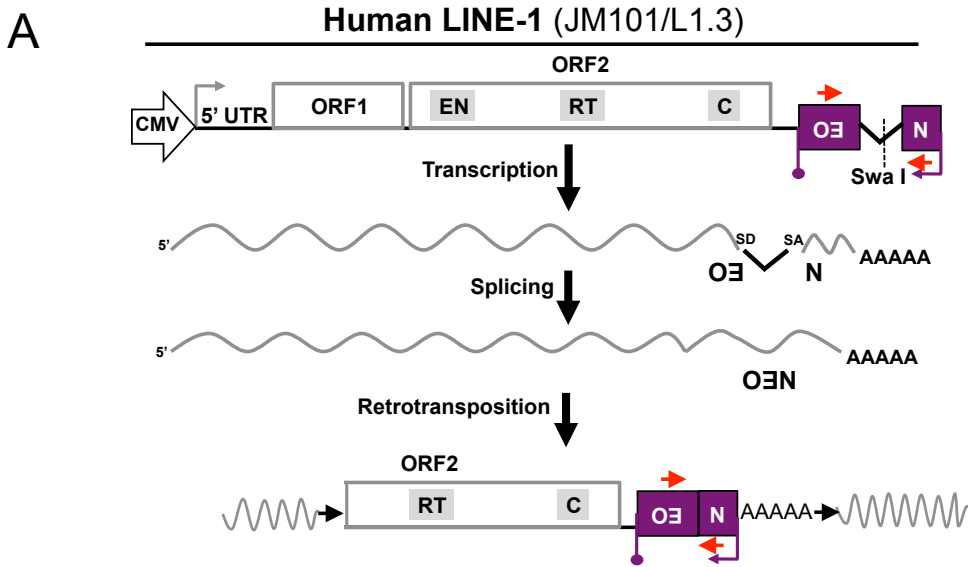
E

RNase H2	Total analyzed	Mutated	% Mutated
+	67	27	40
-	69	26	38

A
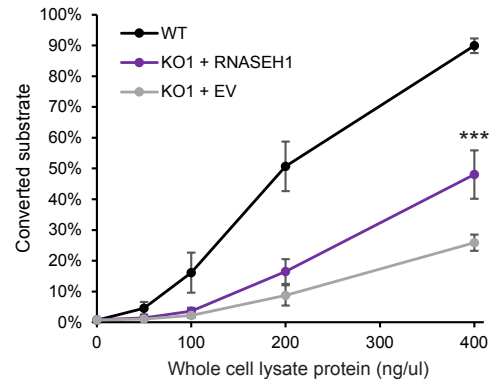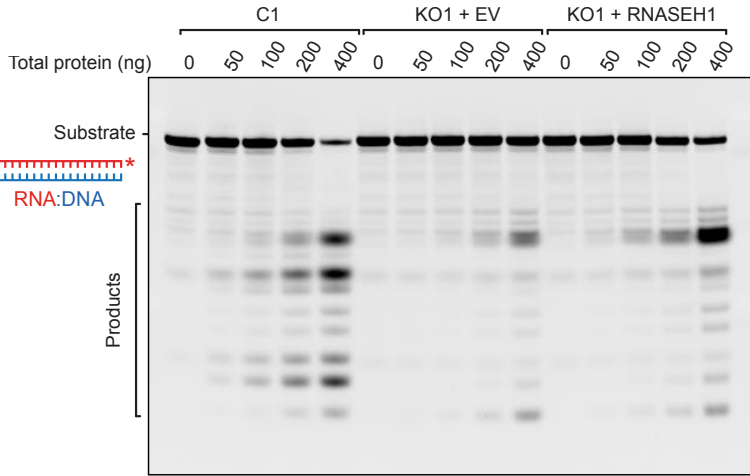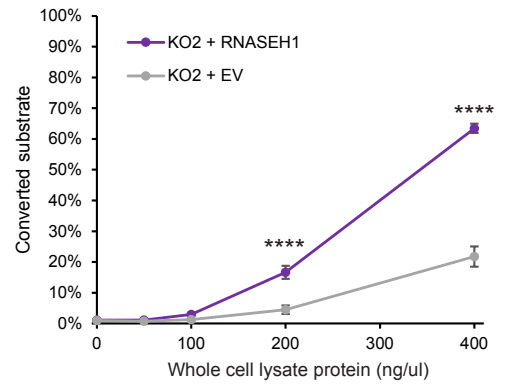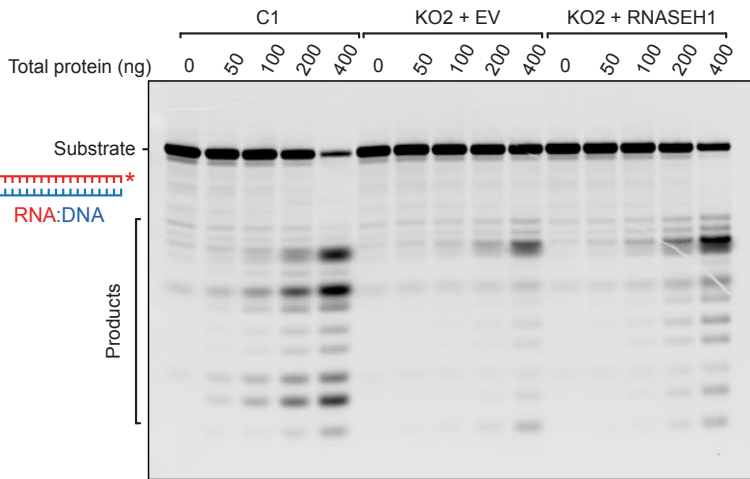
Appendix Figure S4

B

Source Data Figure 1

α-RNASEH2A (SC)

RNASEH2A

α-Tubulin

Tubulin

α-RNase H2 (short exposure)

RNASEH2B

α-RNase H2 (long exposure)

RNASEH2C

Source Data Figure 2

α-RNASEH2A

RNASEH2A

α-RNase H2 (short exposure)

RNASEH2B

α-RNase H2 (long exposure)

RNASEH2C

α-Vinculin

Vinculin

Source Data Figure 5

α-RNASEH2A (SC) α-RNase H2 (short) α-RNase H2 (long) α-Tubulin

RNASEH2A RNASEH2B RNASEH2C Tubulin

Source Data Figure 7

α-RNASEH2A (SC)	α-RNase H2 (short)	α-RNase H2 (long)	α-Actin
RNASEH2A	RNASEH2B	RNASEH2C	Actin
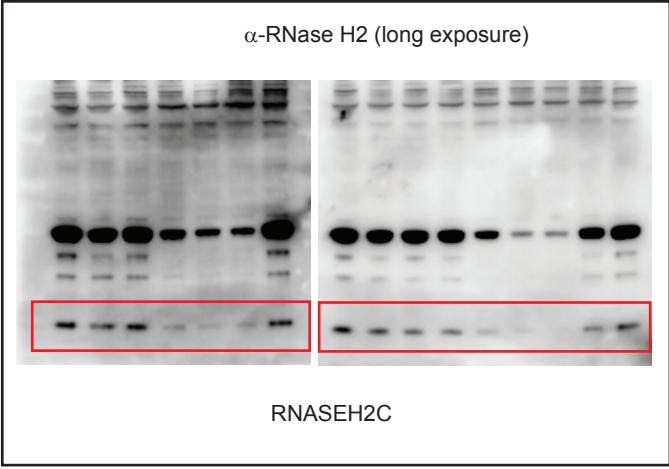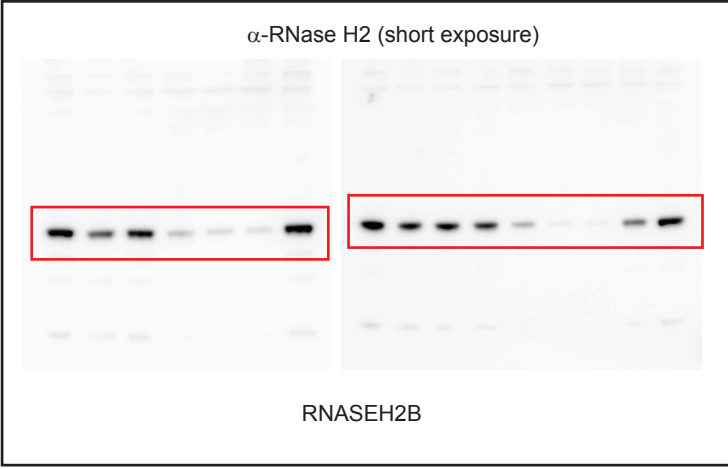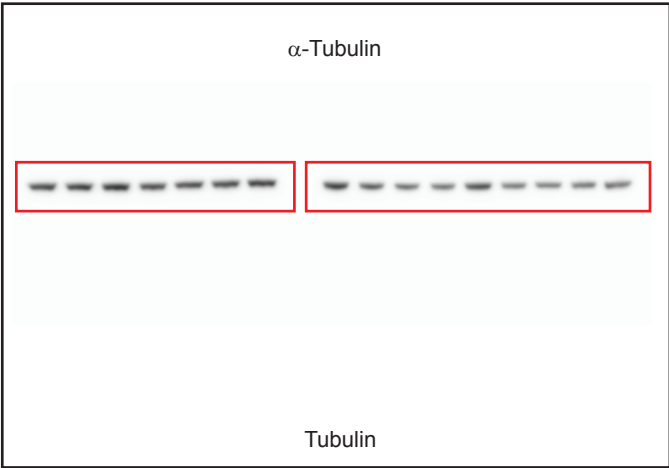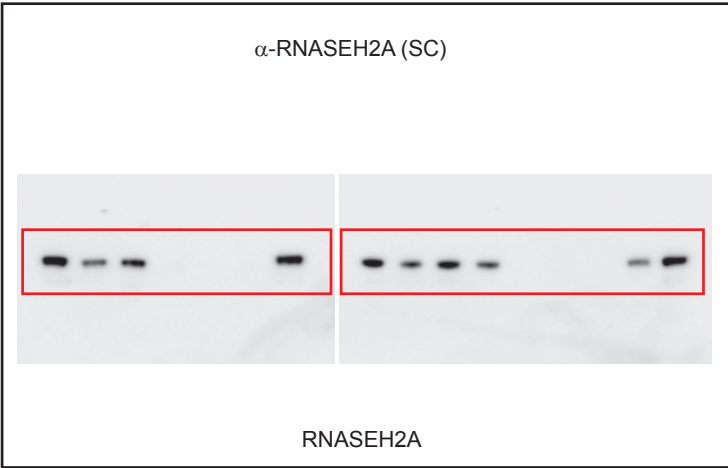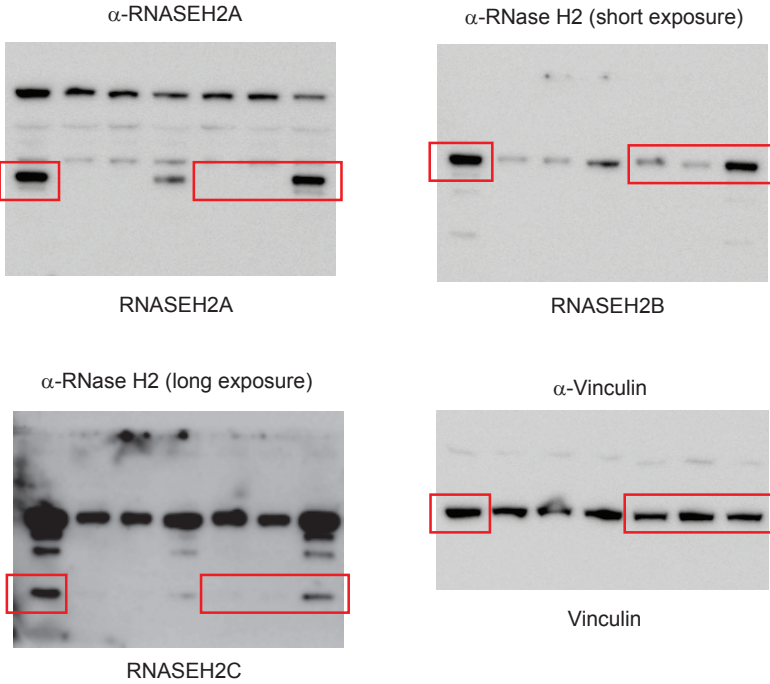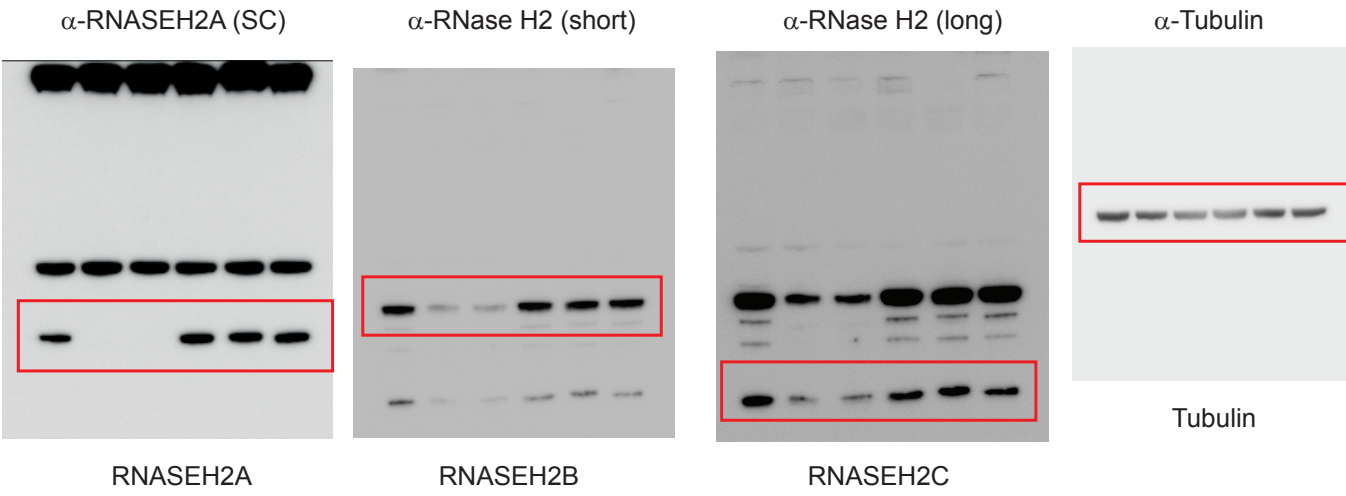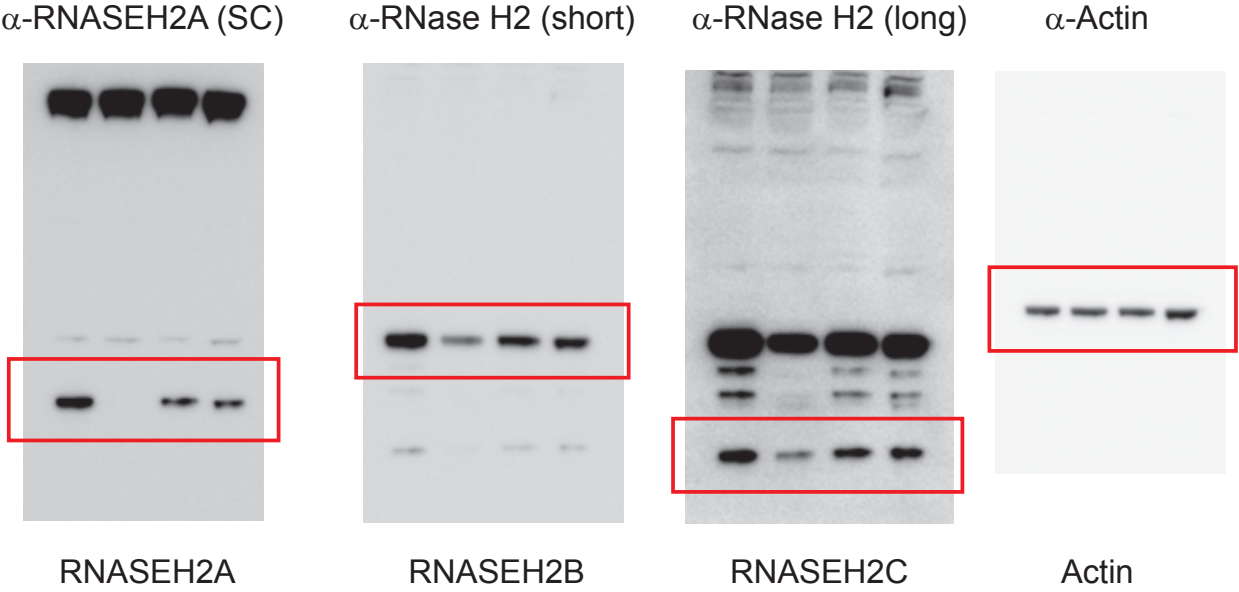
Source Data Figure EV1

Source Data Figure EV3

V5-RNaseH2
A+B+C

V5-RNaseH2

A   B   C   1:1:1   14:7:1   UTF

HeLa

β-actin

MW.
kDa

**V5-RNaseH2**
A+B+C

V5-RNaseH2

A   B   C   1:1:1   14:7:1   UTF

U2OS

β-actin
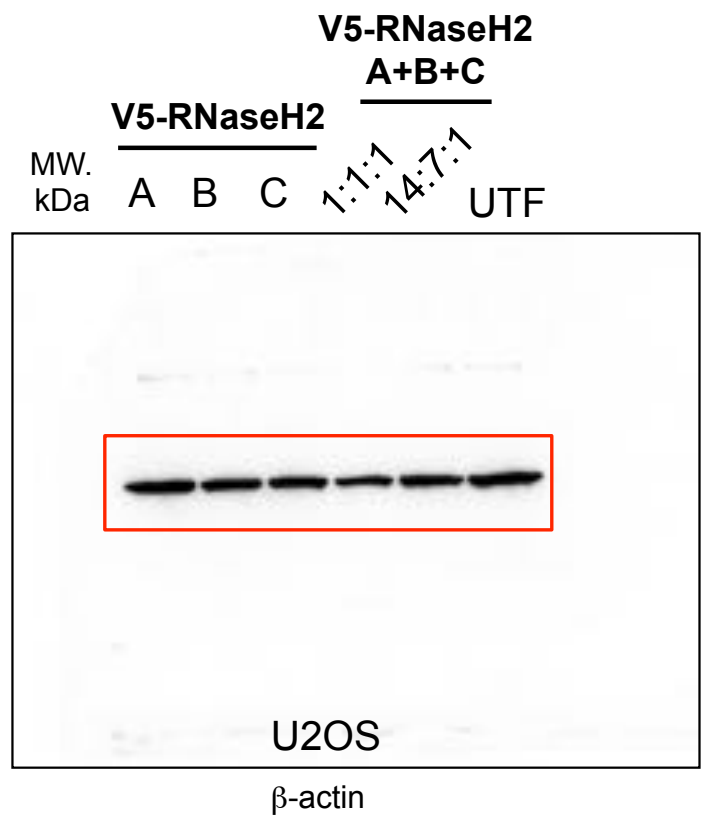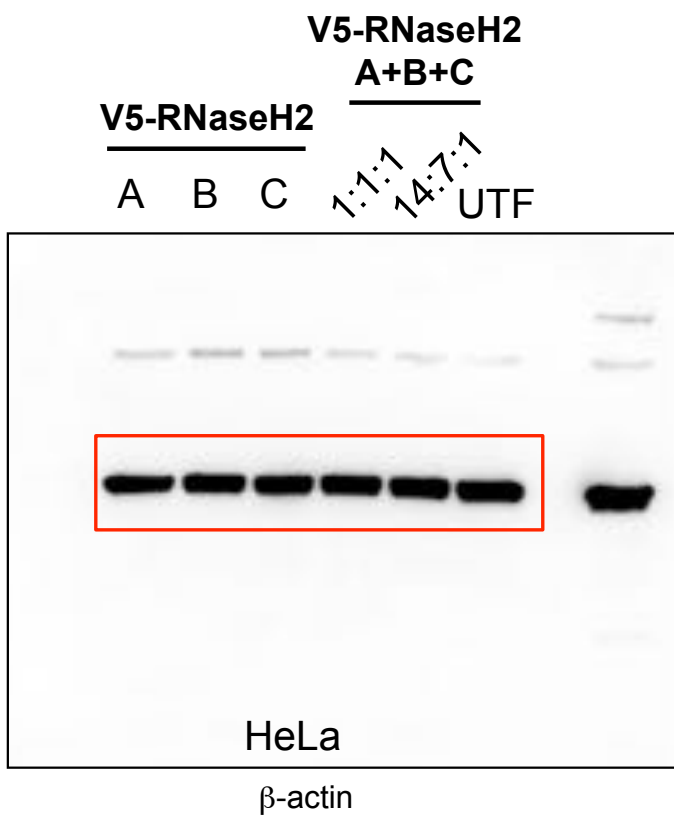
Source Data Appendix Figure S1

α-RNASEH2A	α-RNase H2 (short)	α-RNase H2 (long)	α-Tubulin
RNASEH2A	RNASEH2B	RNASEH2C	Tubulin